COMBINED FLOW AND HEAT TRANSFER CHARACTERIZATION OF OPEN CELL ALUMINUM FOAMS

By

Ángel R. Álvarez Hernández

A thesis submitted in partial fulfillment of the requirements for the degree of

MASTER OF SCIENCE

In

MECHANICAL ENGINEERING

UNIVERSITY OF PUERTO RICO
MAYAGÜEZ CAMPUS
2005

Approved by:

_____	_____
Sandra Coutín Rodicio, Ph.D. Member, Graduate Committee	Date
_____	_____
Gustavo Gutiérrez, Ph.D. Member, Graduate Committee	Date
_____	_____
Nihad Dukhan, Ph.D. President, Graduate Committee	Date
_____	_____
Basir Shafiq, Ph.D. Representative of Graduate Studies	Date
_____	_____
Paul Sundaram, Ph.D. Chairperson of the Department	Date

ABSTRACT

The use of open-cell metal foams have been widely increasing given by its diverse novel properties in various areas including aerospace, electronics and automotive among others. They are a relative new class of materials with very promising applications in which it's low density, high surface area to volume ratio and other thermal, mechanical, electrical and acoustical properties make this material an excellent means for performance improvement. Important applications have been found taking advantage of the thermal properties of the metal foam. These applications include compact heat exchangers for airborne equipment, air-cooled condenser towers, both the regenerative and the dissipative type, and compact heat sinks for power electronics. The low relative density, open porosity and high thermal conductivity of the cell edges, the large accessible surface area per unit volume, and the ability to mix the cooling fluid, all make metal foam heat exchangers efficient, compact and light weight. Although it is proven to be very promising, still the use of the open-cell metal foams require extensive efforts to achieve a full characterization. It is as an objective in this thesis work to provide new insights to the characterization of the fluid behavior through the foam and its thermo physical properties. This will be found very useful for the use of metal foams in heat transfer and flow applications. Also the use of metal foams as heat sinks in electronic cooling is evaluated, and its advantages and disadvantages are highlighted for future reference.

RESUMEN

El uso de esponjas metálicas esta aumentando notablemente dado a sus diversas y novedosas propiedades en áreas como la aeronáutica, la industria automotriz y la industria electrónica como entre otras. Son relativamente un tipo de material nuevo y prometedor de los cuales sus propiedades como; baja densidad, alta razón de área superficial a volumen y otras propiedades térmicas, mecánicas, eléctricas y acústicas hacen de ellas materiales idóneos para un sinnúmero de usos. Aplicaciones importantes han sido encontradas donde las esponjas proveen una mejoría en desempeño térmico como en intercambiadores de calor compacto para equipo aéreo, torres de condensado por aire, y equipo para enfriamiento de componentes electrónicos de alto redimiendo. Sus propiedades y su habilidad de mezclar los fluidos hacen de las esponjas excelentes materiales para el uso de intercambiadores de calor creando sistemas compactos, eficientes y livianos.

Aunque han probado ser prometedores por sus características, siguen siendo muy necesarios los esfuerzos para caracterizar completamente este tipo de material. Como parte del objetivo de este trabajo de investigación se proveerá información sobre el comportamiento del fluido a través del medio y sus propiedades termo físicas. Esta información será de mucha utilidad para el uso de esponjas de metal en aplicaciones de flujo o transferencia de calor a través del medio. En adición el uso de esponjas de metal para aplicaciones de enfriamiento de equipo electrónico será evaluado, y sus ventajas y desventajas serán resaltadas para referencia futura.

DEDICATION

To my family who has always given me support to pursue my dreams. To my loving daughters Coralis and Alejandra to whom I owe the motivation needed in this journey and to my good friends Sonja Mongar and Melvin López who believed in me and inspired me to achieve this goal.

To Yesenia Hernández, thank you for your patience and understanding.

ACKNOWLEDGEMENTS

I would like to give thanks to Dr. Nihad Dukhan for all his good advice the Mechanical Engineering Department and Dr. Miguel Velez for providing me with the support to complete this work.

TABLE OF CONTENT

ABSTRACT ii

RESUMEN iii

DEDICATION iv

ACKNOWLEDGEMENTS v

TABLE OF CONTENT vi

TABLE LIST viii

FIGURE LIST ix

FIGURE LIST ix

NOMENCLATURE xii

Greek symbols xiv

CHAPTER 1 Introduction 1

1.1 Background 1

1.2 Foams 2

1.3 Categorization of Metal Foams 3

1.4 Production of the Duocell samples and final geometry 5

1.5 Aplications 10

1.6 Research Overview 11

CHAPTER 2 Literature Review 13

CHAPTER 3 Fluid Flow and Pressure Drop in Aluminum Foams 21

3.1 Introduction 21

3.2 Equipment 26
3.3 Experiment 31
3.4 Results 34
3.5 Empirical Model 49
3.6 Conclusions 52
CHAPTER 4 Forced Convection in Metal Foams 54
4.1 Introduction 54
4.2 Equipment 56
4.3 Experimental Procedure 58
4.4 Results 64
4.5 Conclusions 66
CHAPTER 5 Thermal Management using Metal Foams 68
5.1 Introduction 68
5.2 Equipment 73
5.3 Experiment 76
5.4 Results 77
5.5 Conclusion 87
REFERENCES 89

TABLE LIST

Table 3-1 Metal foam sample properties 28

Table 3-2 Experimental velocity and pressure ranges 35

Table 3-3 Metal foam flow parameters for different Reynolds ranges..... 40

Table 3-4 Permeability based Reynolds range for each sample 41

Table 4-1 Empirical coefficients..... 66

Table 5-1 Heat sink metal foam properties..... 74

Table 5-2 Pressure and velocity ranges obtained in the experimental runs..... 77

Table 5-3 Dimensions of the commercially available and the metal foam heat sinks..... 79

Table 5-4 Weight comparison among commercially available 82

Table 5-5 Fan operation data 83

Table 5-7 Heat transfer coefficient based on fan curve 85

FIGURE LIST

Figure 1.1 Open cell metal foam sample 4

Figure 1.2 Closed cell metal foam 5

Figure 1.3 Open cell metal foam manufacturing process 6

Figure 1.4 Metal foam structure..... 7

Figure 1.5 Representative geometry 7

Figure 1.6 10, 20 & 40 PPI metal foam samples 8

Figure 1.7 Metal foam compact heat exchanger..... 11

Figure 3.1 Duocell metal foam samples 26

Figure 3.2 Samples of the structure of compressed and uncompressed metal foams. Uncompressed metal foam samples (a and b). Compressed metal foam samples (c and d) 27

Figure 3.3 Dimension of the metal foam used. 28

Figure 3.4 Air duct used in the experimental work 30

Figure 3.5 Schematic of the air duct 31

Figure 3.6 Cross section of the sample in the air duct and vertical distributions of dynamic pressure vertical points..... 33

Figure 3.7 Normalized pressure drop and air velocity..... 36

Figure 3.8 Length normalized pressure drop vs air velocity for both 2 and 4 inch 40 PPI samples..... 36

Figure 3.9 Length normalized pressure drop vs air velocity for 10, 20 and 40 PPI 2 inch samples..... 37

Figure 3.10 Normalized pressure drop vs air velocity for 10 PPI 2 inch samples and various porosities. 38
Figure 3.11 Normalized pressure drop vs air velocity for 20 PPI 2 inch samples and various porosities. 38
Figure 3.12 Permeability vs Reynolds number for 10, 20 and 40 PPI 2 inch samples with similar porosities. 43
Figure 3.13 Permeability vs Reynolds number for 10 PPI 2 inch samples with different porosities. 43
Figure 3.14 Permeability vs Reynolds number for 20 PPI 2 inch samples with different porosities. 44
Figure 3.15 Inertia coefficient vs Reynolds number for 10, 20, and 40 PPI 2 inch samples with similar porosities. 45
Figure 3.16 Inertia coefficient vs Reynolds number for 10 PPI 2 inch samples with different porosities. 45
Figure 3.17 Inertia coefficient vs Reynolds number for 20 PPI 2 inch samples with different porosities. 46
Figure 3.18 Friction factor vs Reynolds number for 10, 20 and 40 PPI samples with similar porosities. 47
Figure 3.19 Friction factor vs Reynolds number for 10 PPI samples with different porosities. 47
Figure 3.20 Friction factor vs Reynolds number for 10 PPI samples with different porosities. 48
Figure 3.21 Permeability vs Ergun coefficient 51

Figure 3.22 Inertia coefficient vs Ergun coefficient 51

Figure 4.4.1 Minco kapton thermofoil heater 56

Figure 4.2 Experimental set-up for forced convection experiments 59

Figure 4.3 Skematic of the side view of the metal foam sample. 60

Figure 4.4 Temperature distribution in the x direction for the 40 PPI sample for various velocities. 62

Figure 4.5 Convection coefficient vs velocity for the 10 PPI samples 65

Figure 4.6 Convection coefficient vs velocity for the 20 PPI 65

Figure 5.1 Metal foam samples for heat sink applications 73

Figure 5.2 Dimensions of the metal foam heat sinks 74

Figure 5.3 Schematic of air duct used for heat sink metal foams experiments 75

Figure 5.4 Metal foam samples pressure drop vs velocity plot 77

Figure 5.5 Metal foam thermal resistance vs velocity plot 78

Figure 5.6 Metal foam wall convection coefficient vs velocity plot 79

Figure 5.7 Commercially available heat sinks 80

Figure 5.8 Thermal resistance comparison plot 80

Figure 5.9 Pressure drop vs velocity comparison plot 81

Figure 5.10 Convection coefficient vs velocity comparison plot 82

Figure 5.11 Pressure drop vs velocity comparison plot 83

Figure 5.12 Commercially available muffin fan used for comparison 84

Figure 5.13 System curve for the different heat sinks and the characteristics fan curves 84

Figure 5.14 Analytical solution of the solid temperature distribution in the metal foam. 87

NOMENCLATURE

A	curve fit viscous term
A_c	total cross sectional area
A_{eff}	fin effective area
A_{fin}	fin cross sectional area
B	curve fit inertia term
C	Nusselt correlation coefficient
c_F	inertia coefficient
D	geometrical parameter ratio
D_h	hydraulic diameter
d_l	ligament diameter
dp	pore diameter
f	Fanning friction factor
H	fin height
h	mean wall convection heat transfer coefficient
K	permeability
k_e	effective thermal conductivity
k_f	conductivity coefficient for fluid
k_s	conductivity coefficient for solid part
L	depth of foam sample in flow direction
L_P	wet perimeter
N	number of heating sides of the fin

N_{fin}	number of fins
n	empirical coefficient for Ergun type model
Nu	Nusselt number
m	empirical coefficient for Ergun type model
p_d	dynamic pressure
P	static pressure
P_1	air static pressure before the metal foam sample
P_2	air static pressure after the metal foam sample
PPI	number of pores per inch
Pr	Prandtl number
Re_K	permeability Reynolds number
r	Nusselt correlation exponent
S	fin spacing
t	thickness of foam sample
T_b	temperature at the base of the foam
T_{fm}	average temperature in the foam
T_∞	fluid temperature
T_{avg}	average temperature on the base
v	average duct velocity
V_{ss}	Volume of solid fraction of metal foam
V_{sample}	Total volume of the sample
V_{air}	Volume of air fraction

Greek symbols

α	empirical coefficient for the Ergun type model viscous term
β	empirical coefficient for the Ergun type model inertia term
ε	medium porosity
λ	heat transfer coefficient for fins of uniform cross section
θs	dimensionless solid temperature
ρ	relative density of foam
ρ_a	density of the air
ρ_{foam}	density of the foam sample
$\rho_{material}$	density of the base material of the foam sample
σ	surface area per unit volume of foam
ν	kinematic viscosity of the fluid
ψ	similarity transform
η	non-dimensional transverse coordinate
χ	non-dimensional coordinate in the flow direction

CHAPTER 1 Introduction

1.1 Background

The use of open-cell metal foams have been widely increasing given by its diverse properties in various areas including aerospace, electronics and automotive among others [1,2,3]. They are a relative new class of materials with very promising applications in which it's low density and other thermal, mechanical, electrical and acoustical properties make this material an excellent means of performance improvement.

Among their current applications, open cell metal foams are found useful for the construction of light weight structures, energy absorption devices, currently being used by some vehicle manufacturers, and for various fluid flow and thermal applications which is our interest in this work.

Although it is proven to be very promising, the use of the open-cell metal foams in fluid flow and heat transfer application requires an extensive effort to better understand the behavior of the fluid flowing through its matrix composition and the heat transfer mechanism occurring in the medium.

But before the geometric characteristics of open cell metal foams can be explained it is best to describe the definition of foams and the different foams currently available.

1.2 Foams

Foams are the result of a two phase combination created by various processes most of which include the dispersion of a gas through a liquid without dissolving the gas completely. This is very similar to the emulsion process (combination of two immiscible liquids) but having the difference that a gas phase must exist in the foam. Nine distinct processes have been developed to make metal foams of which five are now used in the commercial fabrication of these materials [1]. They can be divided into four main classes:

1. Those in which the foam is formed by the vapor phase.
2. Those in which the foam is electrodeposited in an aqueous solution.
3. Those which depend on liquid-state processing.
4. Those created in the solid phase.

All of these processes can be used with different metals resulting in a variety of relative densities and cell sizes. Among the different combinations the resulting material can be

of open cell type and others in which most of the cells are closed. The most common or mentioned manufacturing processes in the literature for these types of materials are:

1. Bubbling gas through a molten alloy (Al-Al_2O_3, Al-SiC)
2. By stirring a foaming agent (typically TiH_2) into a molten alloy (tipically an aluminum alloy)
3. Consolidation of a metal powder, generally aluminum alloys, with a particulate foaming agent (TiH_2) followed by heating into the mushy state when the foaming agent releases hydrogen expanding the material (Al, Zn, Fe, Pb, Au).
4. Manufacturing of ceramic molds from a wax or polymer foam precursor, following the burning out of the precursor and pressure infiltration with molten metal powder slurry which is then sintered (Al, Mg, Ni-Cr, stainless stell and Cu).

1.3 Categorization of metal foams

Generally metal foams are categorized in two groups based on the liquid fraction and cell geometry. The liquid fraction of what is considered dry foam is relatively low, typically less than 1% and with film type geometry. This dry foam has such a small liquid fraction that the individual cells can be considered single surfaces in which soap bubbles represent its geometry very well.

Wet Foams, on the other hand, have considerable liquid fraction in the order of 50% or more. These foams are characterized by the formation of three dimensional border geometries. The formation of these three dimensional border geometries subcategorizes the wet foams into open and closed cell metal foams.

The differences between open cell and closed cell metal foams are mainly how the geometry of the cell is formed (See Figs.1.1 and 1.2). In the open cell group the cells are not closed from each other and the flow of other materials through one cell occurs freely to another adjacent cell. This type of foam is generally created during the foam manufacturing by removing the inter-cellular membranes of closed cell foam [1].

Figure 1.1 Open cell metal foam sample

In the closed cell arrangement the surface tension and wetness scales increase and the geometry takes a very different shape compared to the open cell arrangements. It is characterized by the continuous cell walls which completely close the cells from one another with the formation of individual cell compartments. The cells nearly take a

spherical shape in these types of metal foams. It is designated as wet foam when the liquid fraction exceeds 5%.

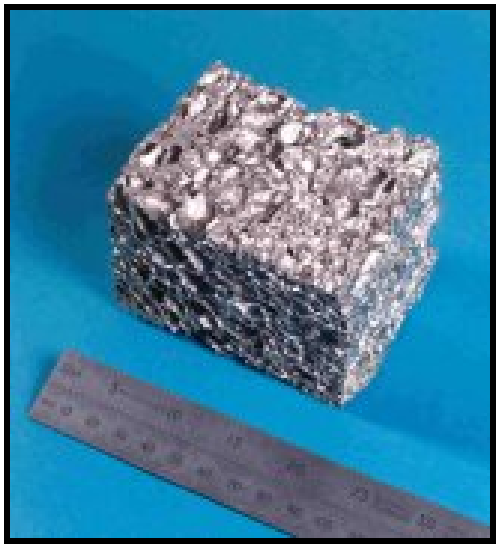

Figure 1.2 Closed cell metal foam

1.4 Production of the Duocell samples and final geometry

The shape and physical characteristics of metal foams vary greatly depending on the manufacturing process used to create them. This has an effect not only on the pore size and porosity but also on the geometry of the pore as well. In the process of an open cell metal foam the resulting material does not take the shape of the molten metal but rather takes the form of a precursor to the metal foam which is usually polymer foam, which is relatively easy to manufacture. For the metal foams samples used in this research (DUOCELL) the process is as follows:

1. Preform- Manufacturing of the open cell polymer foam mold to be used as template with the desired cell size and relative density.
2. Coating- The mold is coated with a mold casting (ceramic powder) which is embedded in casting sand.
3. Burnout- The mold is heated to harden the casting material and decompose the polymer template. This process leaves a negative image of the foam.
4. Infiltration- Metal alloy is poured in the mold and allowed to cool with a moderate pressure during the melt infiltration to overcome resistance to flow of some liquid metal alloys.
5. Removal of mold material- After solidification the mold material is extracted leaving an open cell configuration.

In figure 1.3 a summary of the process is shown.

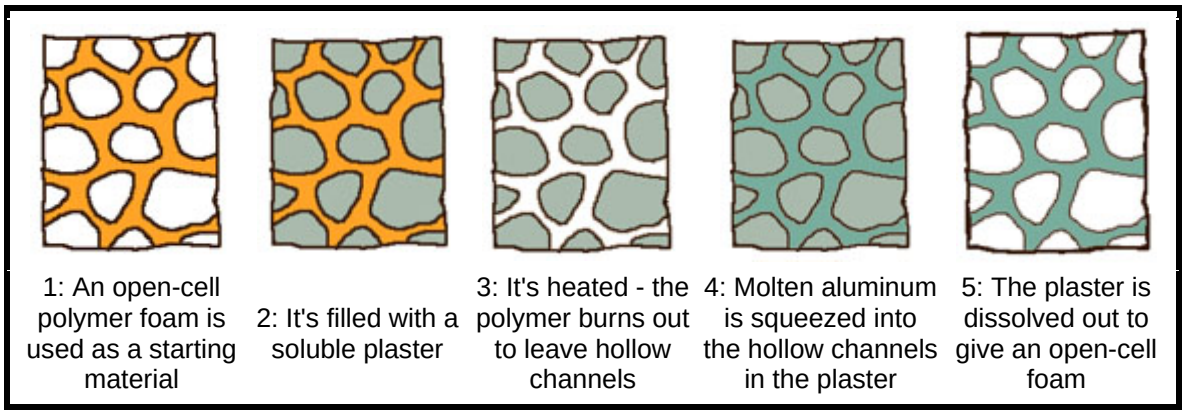

Figure 1.3 Open cell metal foam manufacturing process

After the process is finished the result is open cell metal foam which consists of small filaments that are continuously connected in an open-celled structure. The strength of the foam depends mostly on the base material and the relative density of the foam. Other properties, such as pore size, filament diameter, and cell shape influence certain

foam characteristics, such as the heat transfer and flow characteristics through them. There are various foam parameters commonly known that describe the foam, among these are the pore size and relative density, which are independent of each other. Figure 1.4 shows a picture of the metal foam structures used in this research.

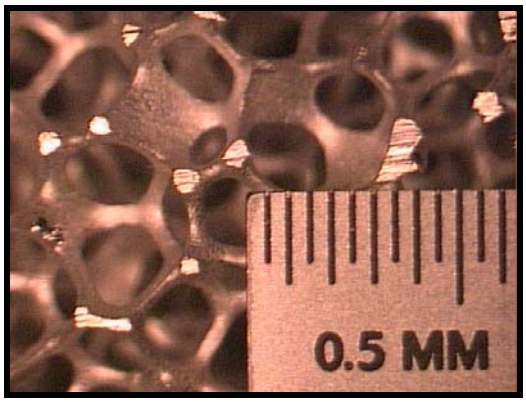

Figure 1.4 Metal foam structure

The cells of metal foam are conformed by polyhedrons (Dodecahedrons) of 12 to 14 faces. Likewise, each face has a pentagonal or hexagonal shape, and therefore, each one is formed by five or six filaments. Figure 1.5 is a very simple representation of the metal foam cell described above.

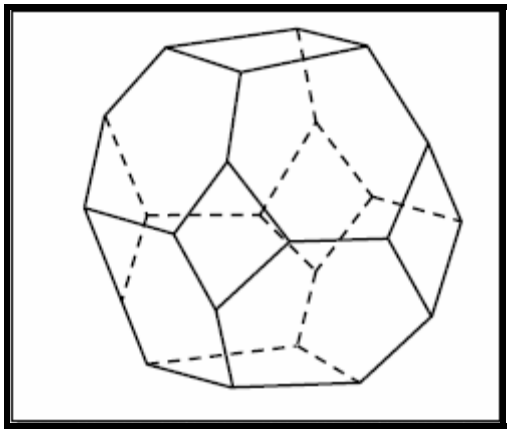

Figure 1.5 Representative geometry

The pore size, one of the most important characteristic of metal foams, is defined by the diameter of one of the faces of the polyhedron cell. The pore density is the number of pores that can be measured in a linear inch and its unit is PPI (pores per linear inch). The available pore densities vary depending upon the base foam material, but their overall uncompressed range is 5-100 PPI. Figure 1.6 shows some samples of open-cell metal foams of different densities.

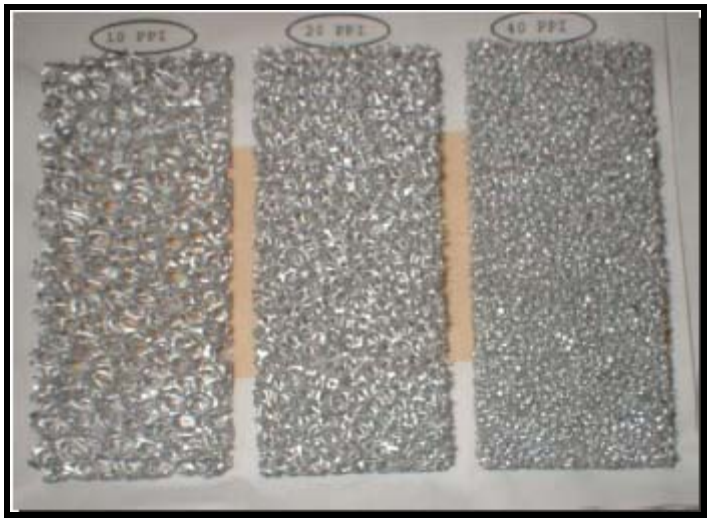

Figure 1.6 10, 20 & 40 PPI metal foam samples

Another characteristic of open cell metal foams is the relative density which is defined as the percentage of solid material. It represents the volume of the solid material relative to the total volume of the foam. It is known that when the relative density is increased, the filaments become larger in diameter and stronger, increasing the strength of the foam structure.

There are various manufacturers known to supply metal foams among them are ERG, Cymat, Recemat, Porvair and even Mitsubishi Materials Japan. Among their

products a variety of materials are used including metals (Aluminum, Copper, and Nickel) and Ceramics. In this experimental work the samples (Duocell) used were manufactured by ERG Corporation in the USA and an aluminum alloy 6101-T6 is used.

The experimental work in this thesis will focus on the fluid flow behavior and heat transfer through a commercially available aluminum 6101-T6 metal foam sample. As it was explained before, metal foam is composed of a porous matrix that consists of tortuous, irregular shaped flow passages. Heat transfer takes place between the surface of the solid matrix and the fluid. The flow re-circulates at the back of the solid fibers. Turbulence and unsteady flows occur when a Reynolds number greater than 100 is presented at the pore-scale. Due to the geometric complexity and the random orientation of the solid phase of the porous medium, the exact solutions of the transport equations inside the pores are difficult to obtain.

Although efforts are still necessary and it is one of this Thesis objective, a number of studies have been conducted by various authors as a means to characterize metal foams. A literature review will be discussed in the next chapter of this Thesis.

In this work a fluid flow and heat transfer characterization will be conducted for various samples of open cell metal foams of a variety of pore densities and porosities.

1.5 Applications

Metal foams have been used as lightweight supporting structure in aerospace applications, especially in the cryogenic field [1, 2]. Different types of metal foams are used as cladding on buildings, strain isolation and as a buffer between a stiff structure and a fluctuating temperature field. They are also used in geothermal operations and in petroleum reservoirs [4]. Ceramic foams are used in advanced burners and heat pipes. And nickel foams have been used to improve the performance of high-power batteries, such as those used in lightweight cordless electronics [5]. Thermal management applications of foams include compact heat exchangers for airborne equipment, air-cooled condenser towers, both the regenerative and the dissipative type, and compact heat sinks for power electronics [6]. The open porosity, low relative density and high thermal conductivity of the cell edges, the large accessible surface area per unit volume, and the ability to mix the cooling fluid by promoting eddies [7]; all make metal foam heat exchangers efficient, compact and light weight.

Focusing on the open–cell foams made out of metal, especially aluminum; it is found that they have been used to construct fluid flow control devices as gas diffusers and mixers as well as separators of liquid and gas. The capacity of the metal foams to absorb a great quantity of energy produced by impact when they are used in materials type sandwich is well known. So, the stress-strain response of metal foams can be customized for some specific applications varying the density and alloy of the foam, while its isotropic properties provide identical response without considering the impact

angle.

As previously mentioned, one of the most important applications of the aluminum metal foams is to build compact heat exchangers. The high surface area to volume ratio allows a more compact design than provided by any other materials. A compact heat exchanger made using aluminum metal foam can be observed in Figure 1.4.

Figure 1.7 Metal foam compact heat exchanger

1.6 Research Overview

In this research fluid flow and heat transfer characterization of 6101-T6 aluminum open cell metal foams will be conducted since given its various uses in different

applications these kinds of materials are still incompletely characterized. Pressure measurements will be made in order to characterize the samples and obtain the pertinent flow parameters. Also a semi empirical model (Ergun Type Model) will be obtained with the data gathered. In the heat transfer experimental work of this thesis the wall convection coefficient will be obtained for the different samples and Nusselt correlation will be given with the data. Finally the use of metal foams will be evaluated and comparison made to some commercially available heat sinks in order to prove the use of these materials as heat transfer promoters for the application of cooling electronics.

CHAPTER 2 Literature Review

Metal foams are recognized for being materials in which its diverse properties have an enhancement for heat transfer application due to their novelty and random structure. Many researchers have experimented with metal foams in order to pursue a complete characterization of this kind of materials. But still more efforts are needed in order to fully understand the behavior of these materials in heat transfer and fluid flow applications. In this chapter a summary of the related research made with metal foams will be discussed. Among the literature found, two areas could be identified which are related to this experimental work; fluid flow and heat transfer experimental work.

Starting with what has been found in the literature regarding Fluid Flow characterization, in 1997, Antohe et al. [8] for the purpose of using porous materials in use for heat exchanger applications, specifically to develop a heat exchanger composed of mechanically compressed micro porous matrix for cooling high frequency micro wave systems. He experimented with nine 40 PPI compressed matrices with different compression ratios for a full hydraulic characterization with air and poly—alpha olefin fluid in which porosity (ϕ), permeability (K) and what the author calls the Forchheimer coefficient (c_F) are calculated. The use of a curve fit is used on this experimental work to find the hydraulic parameters in difference with earlier publications in which an extrapolation of the pressure vs velocity graphs are made in order to find the first and second order coefficients in the Forcheimer Eq. (2.1.1) resulting in lower uncertainty values.

$$\frac{\Delta P}{L} = \frac{\mu}{K} v + \frac{c_F}{\sqrt{K}} \rho v^2 \qquad (2.1.1)$$

It was observed that the pressure drop was more sensitive to changes in compression ratio at high flow speeds. The hydraulic behavior of a compressed matrix seemed to become insensitive to changes in the initial matrix density beyond a certain threshold value. For compression ratio equal to 7 the threshold initial density is close to 6%. The permeability of the matrix decreased with an increase in initial aluminum matrix density and with the increase of its compression ratio. The Forchheimer coefficient did not have a monotonic variation. It presented, however a general tendency to increase with increased compression ratio and matrix density. Finally it was noted that unless one is certain that the flow regime is only linear calculating the permeability of the medium from one data point is improper and under estimates the value by a large fraction. That is imperative to provide the range in which the coefficients were calculated and last when using air as the fluid one concern is achieving a Knudsen effect in the low end velocity spectrum of the experimentation. As described by Kaviany [6], at low pressure and small pore size a velocity slip can occur as the mean path of the gas molecules approaches the pore dimension. This "slippage" effect reveals itself as an increase in the flow rate as the pressure gradient was decreased, a fact that leads to an apparent higher permeability.

Later in 1997 Lage and Antohe [9], performed new experiments with 40 PPI samples in order verify what other authors reported in the literature as a decrease in

pressure drop gradients beyond the second order Forchheimer regime. They found that contrary with experimental results with water and packed bed of spheres, that their results with air and aluminum porous medium layers yielded an increase in static pressure gradient as velocity was increased. They correlated their data and found that a cubic term model fitted best their experimental work.

In 1998, Seguin et al. [10] provided experimental characterization of flow regimes for various porous samples. They wanted to provide the limits to the laminar regime and found that the transition to turbulence for a pore diameter based Reynolds number was 470 which corresponds to a permeability based Reynolds number (Re_K), which is the one used in this experimental work, of 0.093.

Decker et al. [11] provided detailed experimental characterization and numerical modeling of the heat and mass transport properties of highly porous media for solar receivers and porous burners. They used nickel chromium alloy foams for their experimental work. They considered the foam as a pseudo-homogeneous, locally-volume-averaged, medium, where the solid and the fluid phases were treated as an artificial single phase with effective properties. They used an additional pressure drop term in the momentum equations, which depended on the properties of the material. They showed that the models for packed beds did not apply to high porosity mediums like the metal foams.

In 1999, Bastawros et al. [12,13] provided data for heat and fluid flow experimental measurements of cellular metals subject to transverse airflow in the Forchheimer, second order, regime. They performed their experimental work with 30 PPI aluminum foams with porosities in the range of $\varepsilon>90$. It was found that a power law was followed when pressure vs velocity plots were recorded. Also the foam thermal performance was characterized through sets of steady-state experimental measurements. The thermal measurements were correlated with models of the thermal dispersion in porous media. These correlations revealed that the filaments normal to the flow direction transmitted most of the heat flux.

In order to use metallic foams to enhance the efficiency of proton exchange membrane fuel cells, in 2003 Crosnier et al. [14] , did some experimental work with 20 and 40 PPI aluminum samples manufactured by ERG and a 20 PPI stainless steel sample manufactured by PORVAIR with porosities greater than 90%. It was recorded that the transition to the turbulence regime was set to a Darican velocity of 1 m/s. It was revealed that as the pore diameter increased in the samples the value of the permeability increased with decreasing pressure drop. Also as the pore size decreased, the surface area increased resultintg in higher mechanical energy dissipation. The passability was defined as the second order term in the Forchheimer Eq. (2.1.1) which is the ratio of the inertia coefficient to the square root of the permeability. It was noted that as the pore size increased there was more variation in the permeability than the passability given to the fact that the permeability scales well with the square root of the pore size while the

passability scaled well with the pore size. The permeability and the passability were functions of the porosity, pore size, the surface area and the solid structure of the foam.

In 2004 Khayargoli et al. [15] studied the effect of the microstructure of metal foams on the flow parameters. In this study they used samples from different manufacturers which ensured different geometrical forms in their inner structure. They used various samples from RECEMAT and IMI made of nickel and Nickel-Chromium alloys with a ranging porosity of 83 to 90% which resulted in different flow parameter values. It was observed that as the pore size increased the surface area increased creating additional flow resistance. The permeability increased and the inertia coefficient decreased with increasing pore size diameter but did not show any clear relation with the porosity. They mentioned that there was strong influence on the drag force exerted on the fluid by which permeability increased with larger pores in the sample which also contributed to the effect of pressure drop. They finally concluded that although the flow phenomenon in the medium was complex, the flow parameters could be predicted using an Ergun like correlation.

Tradrist et al. [16] investigated the use of aluminum metal foams for compact heat exchangers. The porosities were in the range of $\varepsilon>90$. They experimentally determined the flow parameters (permeability and inertia coefficient) and used an Ergun type correlation between the pressure drop and the fluid velocity.

In 2000, Kim et al. [17] experimented with the impact of porous fins on the pressure drop and heat transfer characteristics in plate-fin heat exchangers. They used six 6101 aluminum alloy foams of 10, 20 and 40 PPI's with different porosities using water as the fluid. Both the friction factor and heat transfer were significantly affected by the permeability and the porosities of the samples foam fins. They used the Darcy number, the geometry and the Reynolds number to correlate the friction factor and they used of the Forchheimer equation for the flow parameters.

Paek et al. [18] did experimental work with aluminum foams of different porosities in the range of $89 < \varepsilon < 96$ % to determine the materials thermo physical properties. At a fixed porosity, increasing the cell size increased the surface area to volume ratio which therefore increased the flow resistance by lowering the permeability and increasing the pressure drop. So it was inferred that the permeability was influenced appreciably by both the porosity and the cell size. The friction factor was correlated with the permeability based Reynolds number. Also in this work the one dimensional conductivity of the material was calculated and the results indicated that it decreased as the porosity increased.

Bhattacharya et al. [5] provided analytical and experimental results for the effective thermal conductivity for high porosity metal foams. They used a range of high porosity materials of $90 < \varepsilon < 98\%$ and 5, 10, 20 and 40 PPI pore densities. The analytical model represented the foam by a two-dimensional array of hexagonal cells. The porosity and the pore density were used to describe the porous media. Experimental

data with aluminum foams using air and water as the fluid media were used to validate the analytical solutions. Their experimental work also made use of the Forchheimer equation to describe the flow parameters.

Also various efforts have been conducted in trying to predict the behavior of the fluid flowing through such highly porous media. Du Plesis et al. [19] based their model on a rectangular representative unit cell to predict the pressure gradients for both Darcian an non-Darcian flows. The model was validated using water and a glycerol solution in foams of 45, 60 and 100 PPI and porosities of $\varepsilon \approx 97\%$.

Some literature, although with not much attention, has taken into account the compression of metallic foams in order to increase the heat transfer characteristics of the material. In addition to the work made by Antohe et al. [8], some examples can be found where 40 PPI compressed foams have been tested for various purposes.

Hwang et al. [4] studied the effects of heat transfer and friction drag in a filled porous duct. The samples used were 40 PPI ERG aluminum foams with a range of porosities of $0.7 < \varepsilon < 0.95$ for which 0.7 and 0.8 porosity samples were achieved by compressing the metal foam of 0.95 porosity. The results of this experimental work showed that both the friction factor and the volumetric heat transfer coefficient increase with decreasing foam porosity at a fixed Reynolds number. It was found that the best thermal performance results were obtained for the 80% porosity sample for a fixed

pumping power. Pore Nusselt number empirical correlations were obtained in terms of the Reynolds number for the various porosities.

Boomsma et al. [20] did some research with aluminum foams of 40 PPI porous densities compressed to various ratios with water as the working fluid. The flow parameters for these samples were obtained with a curve fit of the pressure drop vs velocity data. It was found that the structural differences in the pre-compressed form between the 95% and the 92% metal foams did not have a noticeable effect on the permeability and that similar compression factors had similar weighted effects. Increasing the compression factor decreased the permeability by regular incremental amounts and holding the porosity constant while decreasing the pore diameter decreased the permeability and increased form coefficient. Finally it was found that changing the velocity regime resulted in different values for the flow parameters.

Later with this information, Boomsma et al. [21] found the applicability of heat exchangers for electronic cooling, which dissipate large amounts of heat. Some parameters that described the heat exchangers were evaluated through experiments, which included the hydraulic characterization, the heat transfer performance and a study to determine the most efficient heat exchanger for particular heat transfer necessities. It was seen that the compressed aluminum foams made a significant improvement in the efficiency over several commercially available heat exchangers, which operated under nearly identical conditions.

CHAPTER 3 Fluid Flow and Pressure Drop in Aluminum Foams

This chapter has as an objective to calculate the experimental values of Permeability (K) and inertia coefficient (c_F) in various metal foam samples of different pore densities and porosities in order to aid in the characterization of these materials.

3.1 Introduction

Often the characterization of the pressure drop behavior in porous structures has been conducted using analysis in packed granular or spherical beds [6,22,23,24,25]. Given the structural difference between open-cell metal foams and those used in [6,22,23,24,25] and other past investigations, an effort to characterize the fluid behavior when passing through these tortuous passages is still necessary.

Different models have been developed in the past in order to characterize the flow of fluids through porous medium on a macroscopic scale. The first attempts can be traced back to the publication of Darcy in 1856 [20,26], where he established his known Darcy's Law, which states that the pressure drop per unit length for a flow through a porous medium is proportional to the product of the fluid velocity and the dynamic viscosity. Later Krüger et al. [20,27] added the inverse proportionality constant to the Darcy Law known as the fluid permeability (K), which

is a measure of the resistance the fluid undergoes when passing through a porous medium Eq. (3.1.1).

$$\frac{-dP}{dx} = \frac{\mu}{K} v \tag{3.1.1}$$

The velocities in Eq. 3.11, can be the Darcian velocity which is a velocity based on the cross-section of the wind tunnel or a velocity for which the presence solid phase in the medium is accounted for as given in [20,27]. Any of these velocities can be used to calculate the permeability [6,7,11,20]. However Darcy' law is applicable for relatively slow moving fluids and it has been proved that as the velocity increases a form drag becomes more prevalent and should be considered for an appropriate calculation of the permeability describing the porous medium [11,20]. The effect of the increase drag form coefficient was accounted for the modification of the Darcy-Forchheimer equation by including a second term to Eq. (3.1.1) modifying this to a quadratic equation for the pressure drop relation [9,20].

$$\frac{-dP}{dx} = \frac{\mu}{K} v + \frac{c_F \rho}{\sqrt{K}} v^2 \tag{3.1.2}$$

Decker et al. [11] provided detailed experimentation, characterization and numerical modeling of the transport phenomena of highly porous media where the modified Darcy-Forchheimer equation was used to obtain his results. The addition of the quadratic term in the equation of Darcy-Forchheimer was proved to be applicable for packed beds of spheres for

permeability based Reynolds of 80>Re_K>5 by Dibbs and Edwards [28] and by Fand et al. [7] for randomly packed spheres of various diameters.

Antohe et al. [8] in his experimental work for pressure drop data for airflow through compressed metal foams at high velocities determined that beyond the permeability based Reynolds number of Re_K>80 another term was needed to be included in the Darcy-Forchheimer equation to accurately describe the pressure drop. This finding is in agreement with that of Forchheimer when he studied large sets of hydraulic data from flow through porous media [9,20]. We can compare this data knowing that the permeability is a factor that is dependent on the nature of the medium and not on the fluid itself [6]. In our experimentation it was not necessary to use the cubic equation proposed in Lage et al. [9] and Forchheimers [9,20] since our Reynolds number was between the accepted range for the quadratic term, but it may be necessary for future experimentations.

In the flow characterization of these type of material the Reynolds number is a usual non-dimensional parameter used to indicate the flow regime used in the experimentation. Although various definitions of the Reynolds number have been proposed in the past literature [26], the most accepted definition used at the macroscopic level is the permeability based Reynolds number Eq. (3.1.3), although Lage et al. [26] has proposed another non-dimensional term to describe the ratio of macroscopic form to viscous forces on porous media.

$$\mathrm{Re}_K = \frac{\rho v K^{\frac{1}{2}}}{\mu} \tag{3.1.3}$$

Through experimentation there are various ways to calculate the permeability (K) and the inertia coefficient (c_F). Hwang et al. [4] and Givler and Altobelli [29] in their experiments linearized the Darcy-Forchheimer equation and ploted the data points of the normalized pressure drop vs velocity to obtain the permeability as the slope. Afterwards the inertia coefficient was obtained by extrapolating the data points in order to find the intercept. This method however has been shown to lack accuracy due to the extrapolation. A more direct and accurate way was introduced by Antohe et al. [8] and later used by Bhattacharya et al. [5] and Boomsma and Poulikakos [20] were a Least Square Quadratic curve fit through the pressure-drop vs velocity data points is used. One of the advantages of this method is that it provides the necessary information for an accurate uncertainty analysis needed when experimental work is done. The procedure is as follows.

Given,

$$A = \frac{\mu}{K} \tag{3.1.4}$$

and

$$B = \frac{\rho c_F}{\sqrt{K}} \tag{3.1.5}$$

Making substitution of Eq. (3.1.4) and (3.1.5) in Eq. (3.1.2) yield the following quadratic equation for the length-normalized pressure drop.

$$\frac{\Delta P}{L} = Av + Bv^2 \tag{3.1.6}$$

In Eq. (3.1.6) the coefficients A and B are solved through the least squares curve fit technique. Applying the least square quadratic fit to the above equation gives the following results for A and B.

$$A = \frac{\left(\sum_{i=1}^{n} x_i y_i\right)\left(\sum_{i=1}^{n} x_i^{4}\right) - \left(\sum_{i=1}^{n} x_i^{2} y_i\right)\left(\sum_{i=1}^{n} x_i^{3}\right)}{\left(\sum_{i=1}^{n} x_i^{2}\right)\left(\sum_{i=1}^{n} x_i^{4}\right) - \left(\sum_{i=1}^{n} x_i^{3}\right)\left(\sum_{i=1}^{n} x_i^{3}\right)} \tag{3.1.7}$$

$$B = \frac{\left(\sum_{i=1}^{n} x_i^{2} y_i\right)\left(\sum_{i=1}^{n} x_i^{2}\right) - \left(\sum_{i=1}^{n} x_i y_i\right)\left(\sum_{i=1}^{n} x_i^{3}\right)}{\left(\sum_{i=1}^{n} x_i^{2}\right)\left(\sum_{i=1}^{n} x_i^{4}\right) - \left(\sum_{i=1}^{n} x_i^{3}\right)\left(\sum_{i=1}^{n} x_i^{3}\right)} \tag{3.1.8}$$

In these equations, the x_i*'s* represent the various fluid flow velocities taken in the experimental runs and y_i*'s* represent the normalized pressure drop points. Knowing A and B the permeability and the inertia coefficient can be calculated by back solving Eq. (3.1.4) and Eq. (3.1.5)

The reason to hydraulically characterize the properties of metal foams is to better understand the flow mechanism through them in order to use its novel thermal properties to the application of thermal heat exchangers or heat sinks. It is a common practice used in the industry to increase the exchange surface area of conventional heat exchangers reaching very high values

but increasing the pressure drop of the fluid circulating the porous matrix. Since not much knowledge of hydraulic aspects of this type of porous material is available to this date, it is an area of investigation necessary to determine the optimal parameters of the porous medium in order to maximize the heat transfer, in the design stage for this type of application, with regard to the pressure drop.

3.2 Equipment

The samples used in this experimental work were manufactured by ERG Materials and Aerospace Corporation. There were various samples of the Duocell 6101-T6 aluminum alloy metal foams. Among the various samples there were different porosities, pore densities and dimensions as depicted in Fig. 3.1 and Table 3.1.

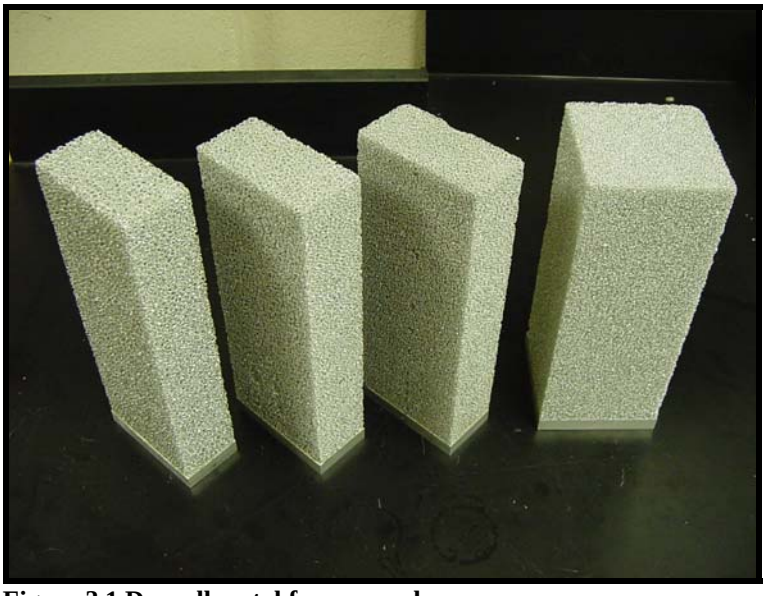

Figure 3.1 Duocell metal foam samples

For some of these samples the porosity was varied by compressing the samples to different compression factors fig. 3.2. The procedure for compressing the foam allows the foam to expand freely on the open lateral sides of the compression device. By not restraining the lateral edges of the foam block while being compressed, the isotropicity of the aluminum is claimed to be held more consistent by avoiding mass accumulation along the edges.

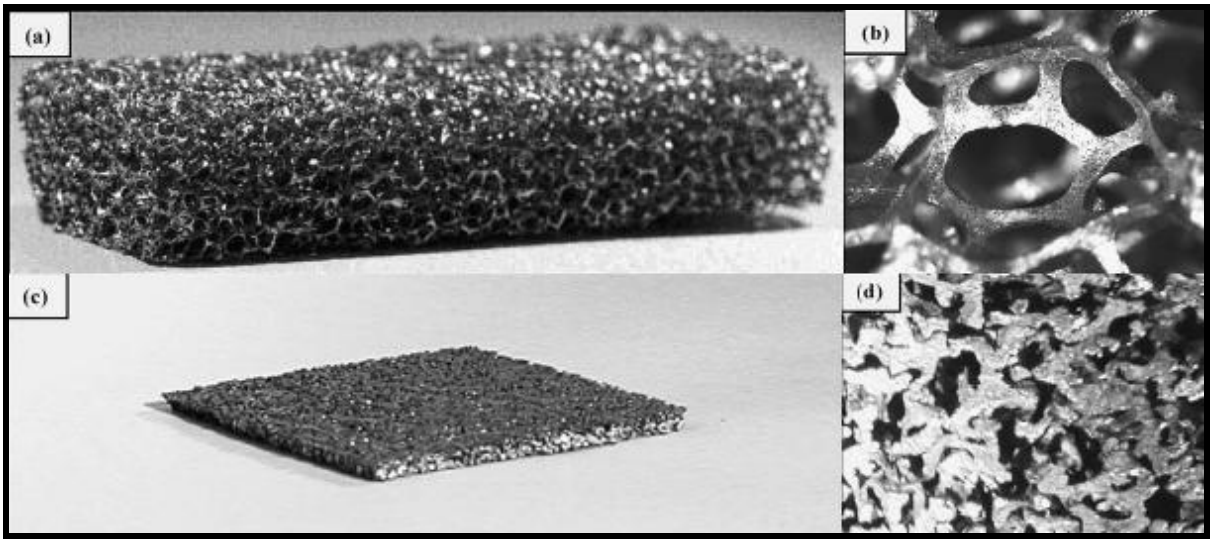

Figure 3.2 Samples of the structure of compressed and uncompressed metal foams. Uncompressed metal foam samples (a and b). Compressed metal foam samples (c and d)

In this experimental work the samples used had dimension similar to the ones depicted in fig. 3.2 and will be designated below by the Height, Width, and Depth (H x W x D). All of the samples had an aluminum base brazed to the metal foam.

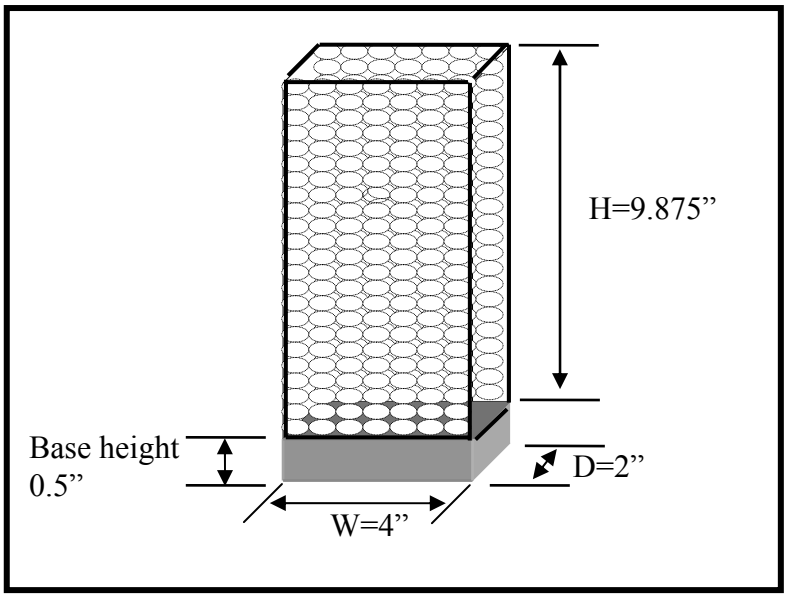

Figure 3.3 Dimension of the metal foam used.

Table 3-1 Metal foam sample properties

No.	PPI	ε	d_L(mm)	d_p(mm)	Size (in) (H x W x D)	σ(m^2/m^3)
1	10	0.914	.406	5.08	9.875 x 4 x 2	809.1
2	10	0.794	.406	1.93	9.875 x 4 x 2	2053.1
3	10	0.682	.406	1.24	9.875 x 4 x 2	3169.3
4	20	0.924	.203	2.90	9.875 x 4 x 2	1240.2
5	20	0.774	.203	0.89	9.875 x 4 x 2	3593.7
6	20	0.679	.203	0.63	9.875 x 4 x 2	5104.3
7	40	0.923	.102	1.70	9.875 x 4 x 2	1800.8
8	40	0.918	.102	1.70	9.875 x 4 x 4	1800.8

The porosities and the relative densities of the samples used were calculated with the following procedure. The samples were weighted and its respective mass was obtained. This value was divided by the density of the solid material to obtain the volume of the solid in the sample. The volume of the solid part of the sample (*V*ss) is subtracted from the total volume of the sample to get the volume of the air inside the foam sample. This value is then divided by the total volume of the sample and so the porosity of the foam is obtained.

$$\varepsilon = \frac{V_{air}}{V_{sample}} = \frac{V_{sample} - V_{ss}}{V_{sample}} \tag{3.2.1}$$

Two sets of runs were made in order to separate the results obtained varying the pore density and keeping the porosity at approximately the same values and a second run varying the porosities of the samples.

The air duct used was manufactured by TecQuipment model TD.49. This equipment consists of a rectangular area designed and constructed in sections, clipped tightly together with snap-action fasteners and supported at four points along its length. The duct section is 150 mm wide by 300 mm high inside measurement (6 in x 12in), the cross sectional area of the duct is 0.045 m^2 (0.485 ft^2) and the overall length of the duct section is 290 mm (11.4 in). The duct and its conical inlet are constructed in accordance with British Standard recommendations. Entry and exit duct-sections are separated by a plain center-section which is easily removed. Figure 3.4 is a picture of this equipment.

Figure 3.4 Air duct used in the experimental work

The centrifugal fan is arranged to draw air along the duct and is provided with a throttle slide-plate at the fan delivery for varying the flow rate. The fan delivery is a single-inlet, overcast discharge flanged aperture 90 mm x 90 mm suction aperture approximates of 20 mm in diameter. The motor specifications are as follows: 220/240 V., 1 ph., 50 Hz, 4.6 amps, 2850 rpm directly connected to the fan shaft. Determination of the air-flow rate and the air velocity profiles can be made by pitot-static tubes mounted in a traversing mechanism. Figure 3.5 shows a diagram where the major components of the wind tunnel are indicated.

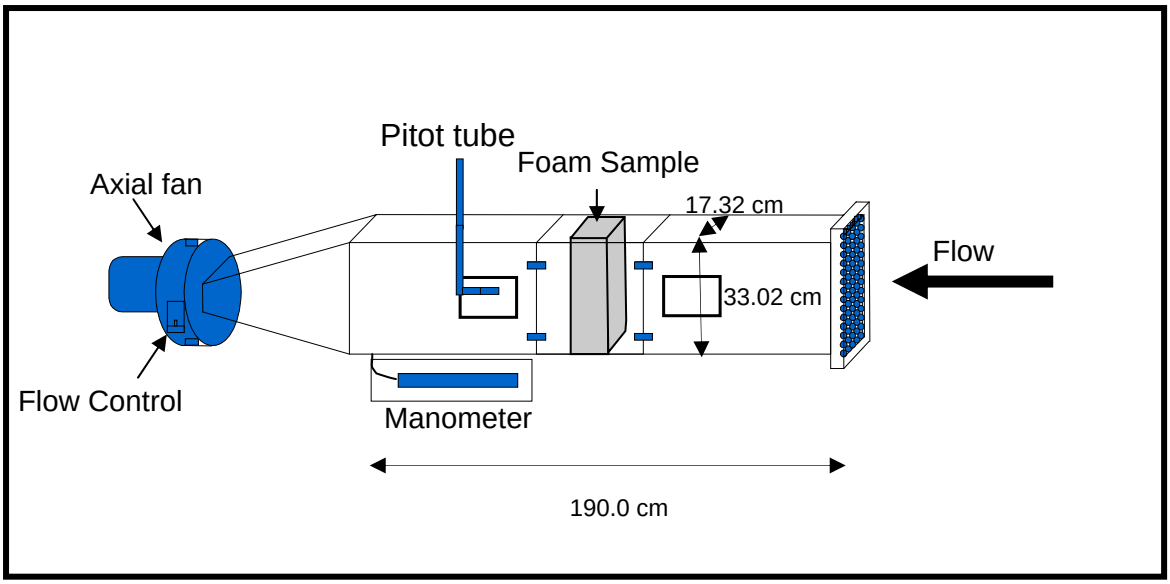

Figure 3.5 Schematic of the air duct

A Pitot tube was used to measure both static and dynamic pressures for the high porosity samples ε>90 for the samples with lower values of porosities a hand held anemometer (Omega HH-30A) was used for the velocity measurements.

3.3 Experiment

As mentioned before the purpose of this experimental section of this work is to determine the flow parameters, permeability (K) and inertia coefficient (c_F) for the samples of metal foam described earlier. These two parameters represent the drag force exerted by the solid ligaments to the fluid. As mentioned earlier these two factors are dependent on the geometry of the porous matrix and independent of the fluid properties.

For this experiment the A TecQuipment multipurpose air duct equipped with a centrifugal fan motor unit, Pitot static probe and inclined tube manometer were used for the

experimentations. Eight samples of metal foam blocks have been tested which include, three samples of 250.825 mm in height, 101.6 mm in width, 5.08 mm of depth and a 12.7 mm brazed aluminum base with 10, 20, 40 PPI's and an additional block of dimensions 241.3 mm in height 101.6 mm in width, 101.6 mm in depth and a 12.7 mm brazed aluminum base with 40 PPI. These samples are described in Table 3.1.

The samples were placed in the wind tunnel and the sides were covered with one inch Styrofoam sheets in order to ensure that all the air flowing through the wind tunnel would only flow through the porous medium of the metal foam. The flow rate in the wind tunnel was varied with a movable plate located at the exit of the centrifugal fan motor. For this experimental procedure the flow rate was varied from 10% to 100% in 10 percent intervals for each foam sample.

Kaviany [4] explains the fluid behavior passing through a porous plug. In this theory the velocity right after the porous medium has practically a constant behavior. Given this information and before the experimentation was conducted, a velocity profile was made taking dynamic pressure readings, at the exit side of the airflow through the porous medium, with the Pitot positioned at various lengths from the sample and at seven vertical points in the sample as shown in fig. 3.8, in order to determine where the velocity profile achieved a more uniform pattern. This is done to reduce the pressure altering effects of the acceleration and deceleration changes of the air after passing through the porous medium. The dynamic pressure readings were taken at ½, 1, 1 ½, 2, 2 ½ and 3 inches from the metal foam samples and at the seven vertical points for 3 different flow rates.

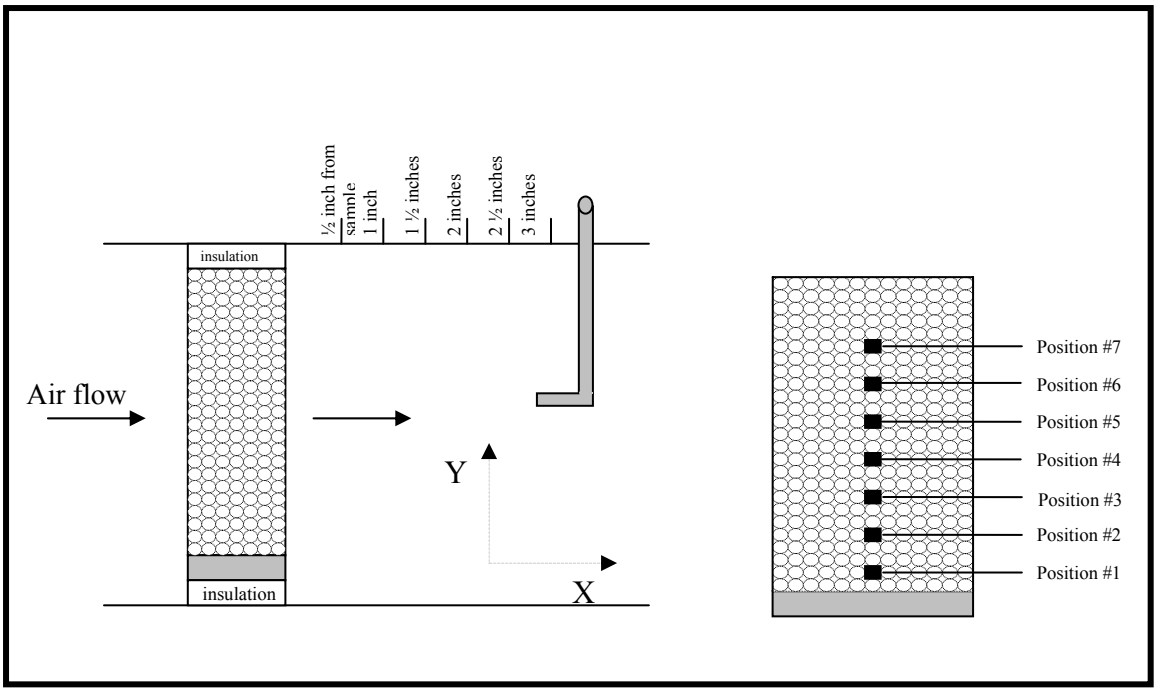

Figure 3.6 Cross section of the sample in the air duct and vertical distributions of dynamic pressure vertical points

Different velocities were obtained at each vertical and horizontal position with Eq. (3.3.1).

$$V = \sqrt{\frac{2P_{dyn}}{\rho}} \tag{3.3.1}$$

After all the velocities were calculated plots of horizontal distance from the sample vs velocity were made for each flow rate. The optimum horizontal distance the Pitot should be placed from the sample to make the static and total pressure measurements was selected by comparing the plots and selecting the distance in which there was less variation in velocity. The resulting distance for these trials was at 1.5 inches from the foam sample.

After the optimum distance was selected, static and total pressure measurements were made for the range of airflow of 10% to 100% in ten percent intervals at the inlet and outlet of airflow passing through the sample. No microscopic pressure changes are taken in this experimentation, only external or macroscopic pressure measurements. With the experimental pressure data obtained for the eight samples, the pressure drop occurring for the airflow passing through the samples was obtained with Eq. (3.3.2) for the different flow rates where P_1 and P_2 are the pressure measurements taken at the inlet and outlet respectively.

$$\Delta P = P_2 - P_1 \tag{3.3.2}$$

After velocity and pressure measurements were obtained for every flow rate and sample, length normalization was calculated with the pressure change with respect to the sample thickness and plotted against the Darcian velocity (v), to obtain the form of the Hazen-Dupuit Darcy modified equation Eq. 3.1.2 when the data is fitted by a least square curve fit to obtain the flow parameters of the foam.

3.4 Results

Pressure measurements were obtained as part of the experimental set-up for each sample of metal foams and plots of macroscopic pressure change vs. air velocity were made. The range for the air velocities and pressure changes were from 0.6340 to 8.6580 m/s and from 526 to

16,450 Pa respectively. In the first runs, it was .727 to 2.764 m/s and 15.92 to 742.60 Pa in the second runs. The ranges for each sample are given in Table 3.2.

Table 3-2 Experimental velocity and pressure ranges

No	PPI	Depth (in)	Porosity	Darcian Velocity range (m/s)	Pressure Range (Pa)
1	10	2	.914	0.83 to 2.76	15.9 to 120.4
2	10	2	.794	0.86 to 2.35	72.7 to 388.7
3	10	2	.682	0.76 to 1.99	126.9 to 590.3
4	20	2	.924	0.77 to 2.72	21.6 to 170.5
5	20	2	.774	0.73 to 1.95	117.1 to 614.8
6	20	2	.679	0.78 to 1.67	209.9 to 472.6
7	40	2	.923	1.0 to 5.46	33.8 to 835.7
8	40	4	.918	0.64 to 4.12	73.0 to 958.4

Figure 3.7 shows a comparison plot of both 2 and 4 inch 40 PPI samples. It could be seen in this plot that the 4 inch sample has basically the same pressure change as velocity is increased compared to the 2 inch sample but clearly it is by the fact that the pressure is normalized with the depth of the sample. It would be evident that the pressure would increase with an increase in velocity with increasing depth and it becomes in a steeper plot with increasing depth Fig. 3.8.

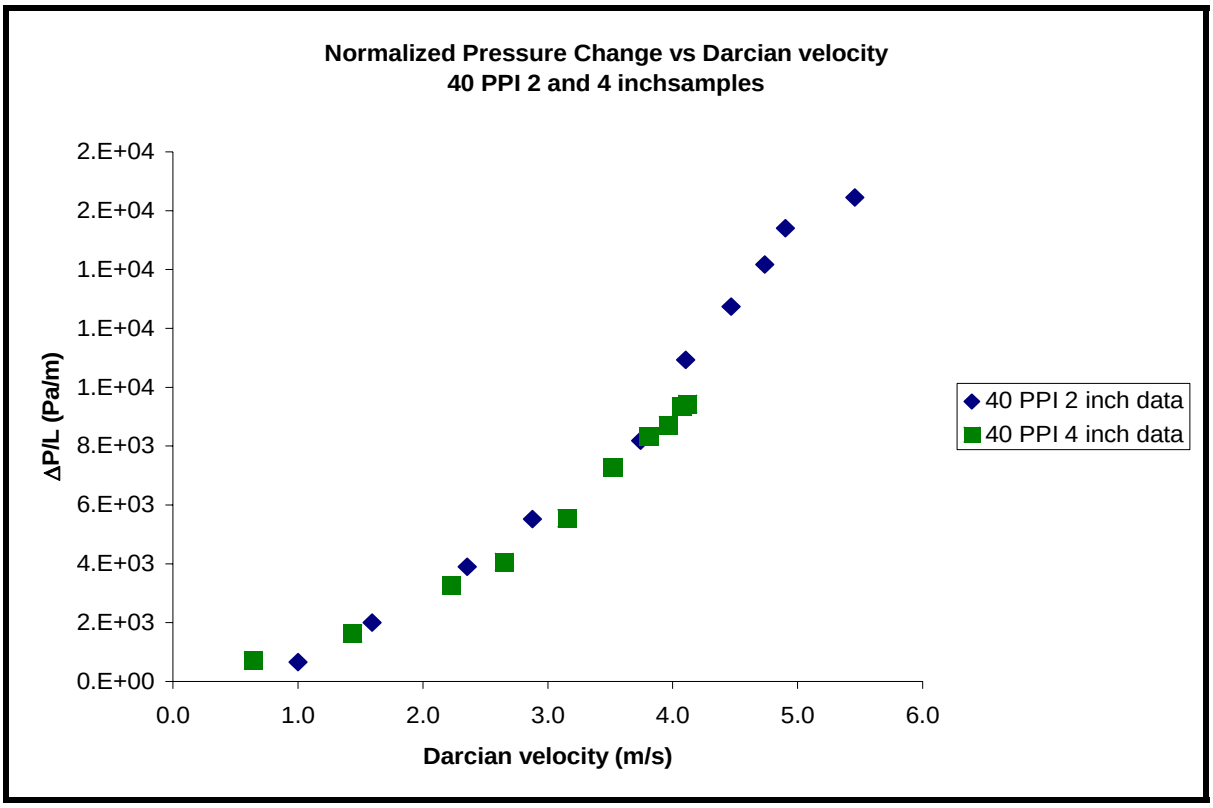

Figure 3.7 Normalized pressure drop and air velocity

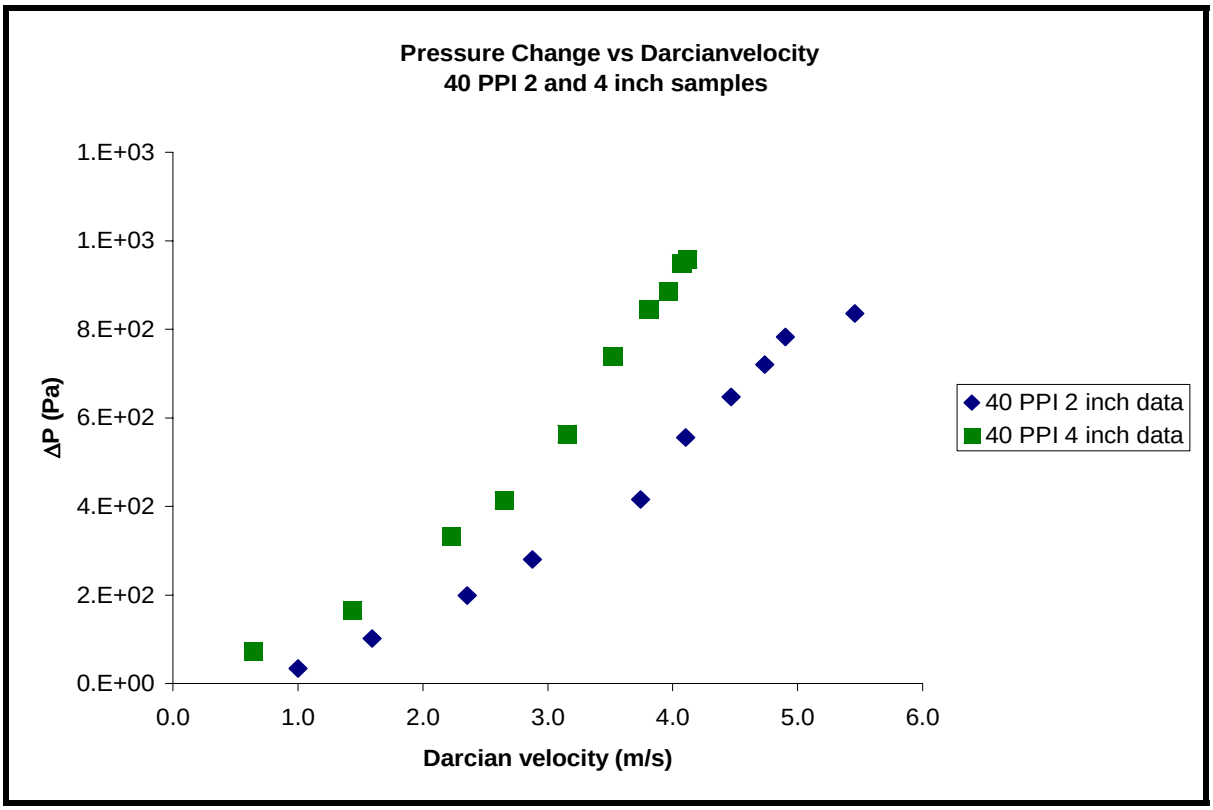

Figure 3.8 Length normalized pressure drop vs air velocity for both 2 and 4 inch 40 PPI samples.

The same plots of normalized pressure change vs Darcian velocity were made for the 10, 20 and 40, 2 inch metal foam samples for each run as shown in Fig. 3.9. It is noted that as the pore density increases, the pressure drop increases with increasing air velocity. This is given by an increase in the tortuosity or obstruction of air flow through the sample. In this graph it must be emphasized that the samples have similar porosity values. The only difference between these samples is the pore density or the average pore diameter of the samples, these varying between 1.702 and 5.080 mm. This difference in pore diameter increased the pressure drop in the medium as it decreased the diameter.

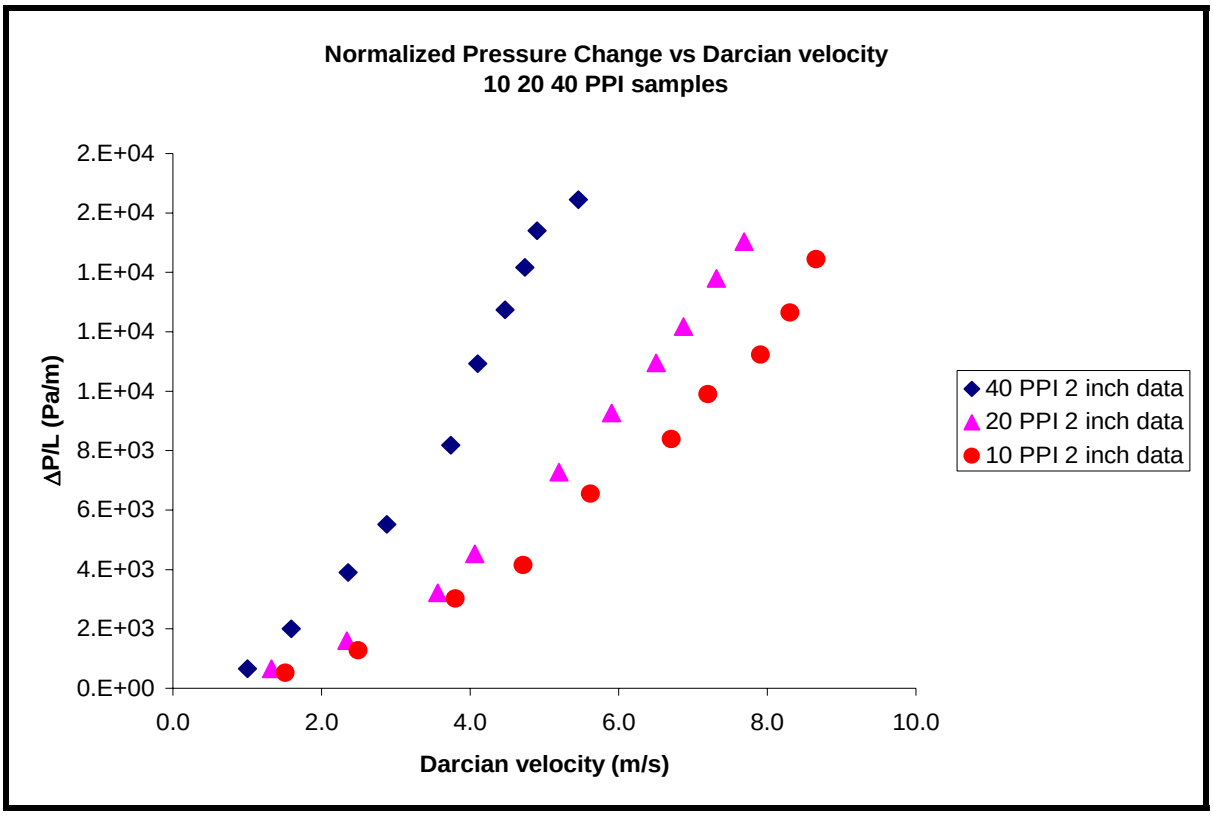

Figure 3.9 Length normalized pressure drop vs air velocity for 10, 20 and 40 PPI 2 inch samples.

In Fig. 3.10 and 3.11 a similar response is obtained when the porosity of the sample is reduced. It is seen that the pressure drop increases with decreasing porosity.

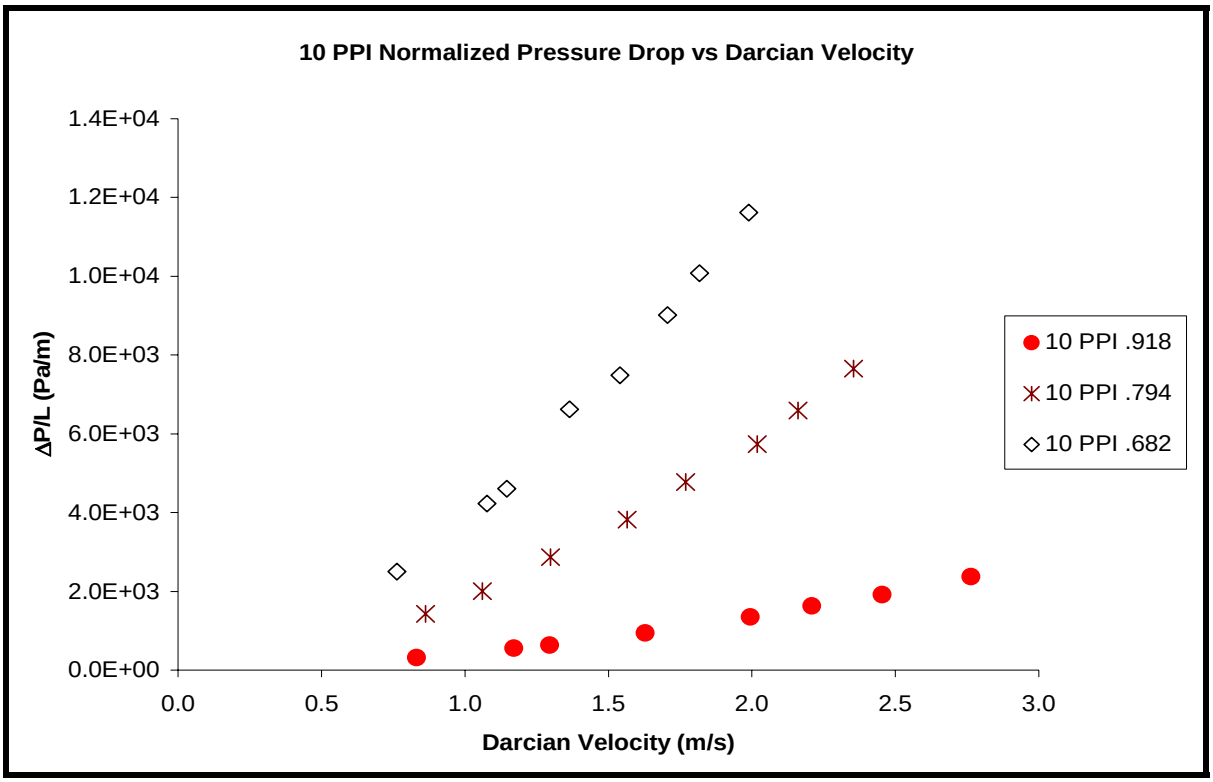

Figure 3.10 Normalized pressure drop vs air velocity for 10 PPI 2 inch samples and various porosities.

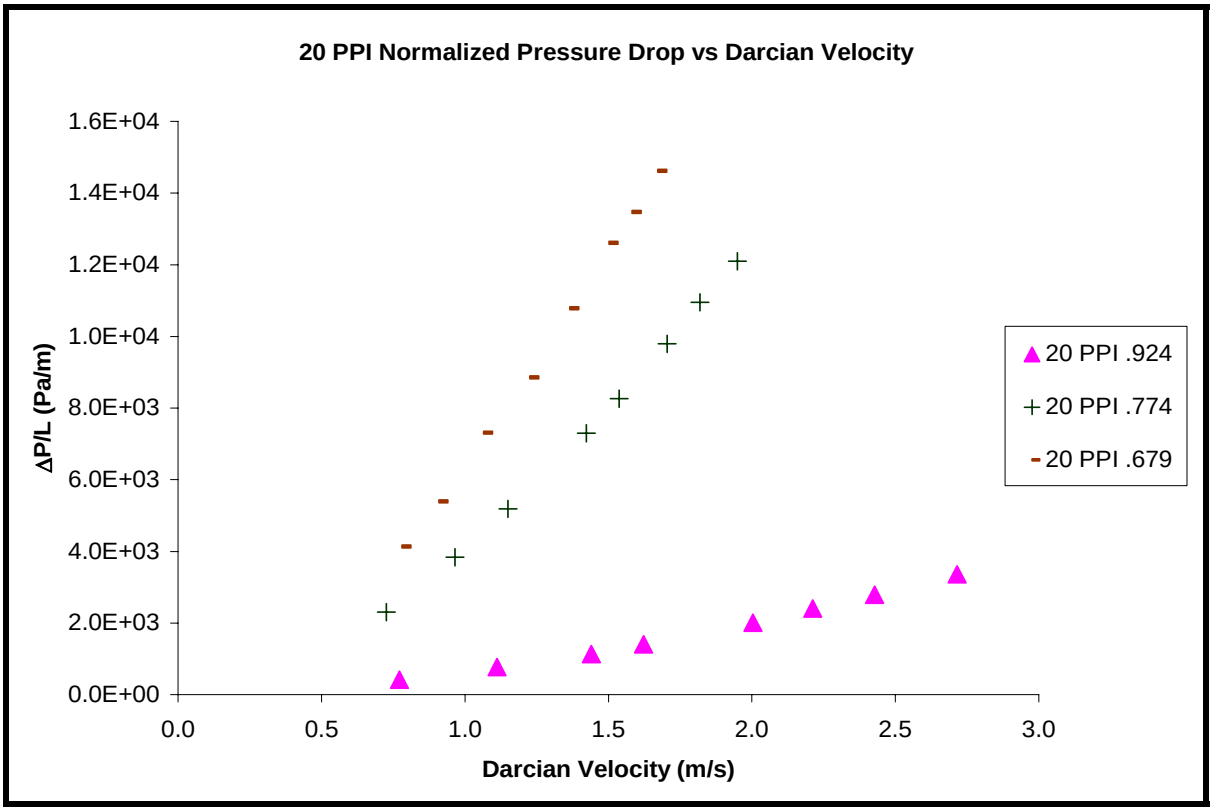

Figure 3.11 Normalized pressure drop vs air velocity for 20 PPI 2 inch samples and various porosities.

There are various ways of calculating the material permeability (K) and the inertia coefficient (c_F). The method of least squares was preferred in this work. This, given its accuracy to curve fit the Length Normalized Pressure Change vs Air Velocity data obtained experimentally. This method was introduced by Antohe et al. [8], and used by many other authors like Boomsma et al. [20].

A quadratic curve fit using the normalized pressure change vs air velocity data obtained experimentally, was made using a spreadsheet. After the quadratic equation was obtained and with the known coefficients, the related flow parameters were obtained with the use of the Hazen-Dupuit-Darcy Eq. 3.4.1.

$$\frac{\Delta P}{L} = Av + Bv^2 \tag{3.4.1}$$

The permeability (K) and inertia coefficient (c_F) for each sample was calculated by back solving for with Eq. 3.4.2 and Eq. 3.4.3.

$$A = \frac{\mu}{K} \tag{3.4.2}$$

$$B = \frac{c_F}{\sqrt{K}} \tag{3.4.3}$$

The results are shown in the following table.

Table 3-3 Metal foam flow parameters for different Reynolds ranges

No	PPI	Depth (in)	Porosity	K (m^2) 10^{-8}	^cF (10^{-1})
1	10	2	.914	10.08	0.70
2	10	2	.794	2.20	1.28
3	10	2	.682	1.04	1.78
4	20	2	.924	6.07	0.72
5	20	2	.774	1.04	1.20
6	20	2	.679	0.68	2.55
7	40	2	.923	3.50	0.79
8	40	4	.918	4.54	0.82

It could be observed from the obtained data that the permeability decreases with pore density and porosity. The value of K is less for the 20 PPI sample compared with the 10 PPI sample also it would be the same response for the 10 PPI sample as the porosity is reduced. This describes how the increasing pore density or decreasing porosity of the sample obstructs the airflow passage through the sample decreasing this way the value of the permeability (K). It is also evident that as the pore density increases or the porosity increases the inertia coefficient increases which is consistent with the physical notion that the more tortuous the passage of air flowing through the sample the greater the inertia forces inside the porous medium increasing this way the value of this coefficient.

This experimental work has been compared with other previous attempts to characterize this type of medium and our results are in agreement with what has been found in the literature. The following tables summarize some results found and compares them to our results.

In the literature relating flow characterization of porous media various definitions of Reynolds numbers have been proposed and used [8,9,20,26]. Among them, particle, interstitial and porosity related Reynolds numbers. But the most popular Reynolds number used in the literature has been the permeability based Reynolds number given by Eq. 3.4.4.

$$\mathrm{Re}_K = \frac{\rho v K^{\frac{1}{2}}}{\mu} \tag{3.4.4}$$

With the experimental velocity data the Reynolds number has been calculated for every airflow interval. The range of Reynolds number used for each sample is given in Table 3.4.

Table 3-4 Permeability based Reynolds range for each sample

No	PPI	Depth (in)	Porosity	Re_K
1	10	2	.914	16.99 to 56.50
2	10	2	.794	8.23 to 22.46
3	10	2	.682	5.01 to 13.07
4	20	2	.924	12.24 to 43.06
5	20	2	.774	4.77 to 12.80
6	20	2	.679	4.13 to 8.85
7	40	2	.923	12.10 to 65.87
8	40	4	.918	8.84 to 56.61

Once again it can be seen that given the higher velocities in the lower densely porous samples higher values of Reynolds numbers.

Another factor obtained with the experimental data was the fanning friction factor obtained with Eq. 3.4.5.

$$f = \frac{\Delta P}{4\left(\frac{L}{D_h}\right)\left(\frac{\rho v^2}{2}\right)} \tag{3.4.5}$$

In Eq. 3.4.5 L is the metal foam depth and D_h is the hydraulic diameter which is obtained with Eq. 3.4.6 where A_c is the cross sectional area and L_p is the wet perimeter of the sample.

$$D_h = \frac{4A_c}{L_p} \tag{3.4.6}$$

With the above information and experimental measurements comparison plots of permeability (K), inertia coefficient (c_F) and friction factor (f) have been plotted as shown below.

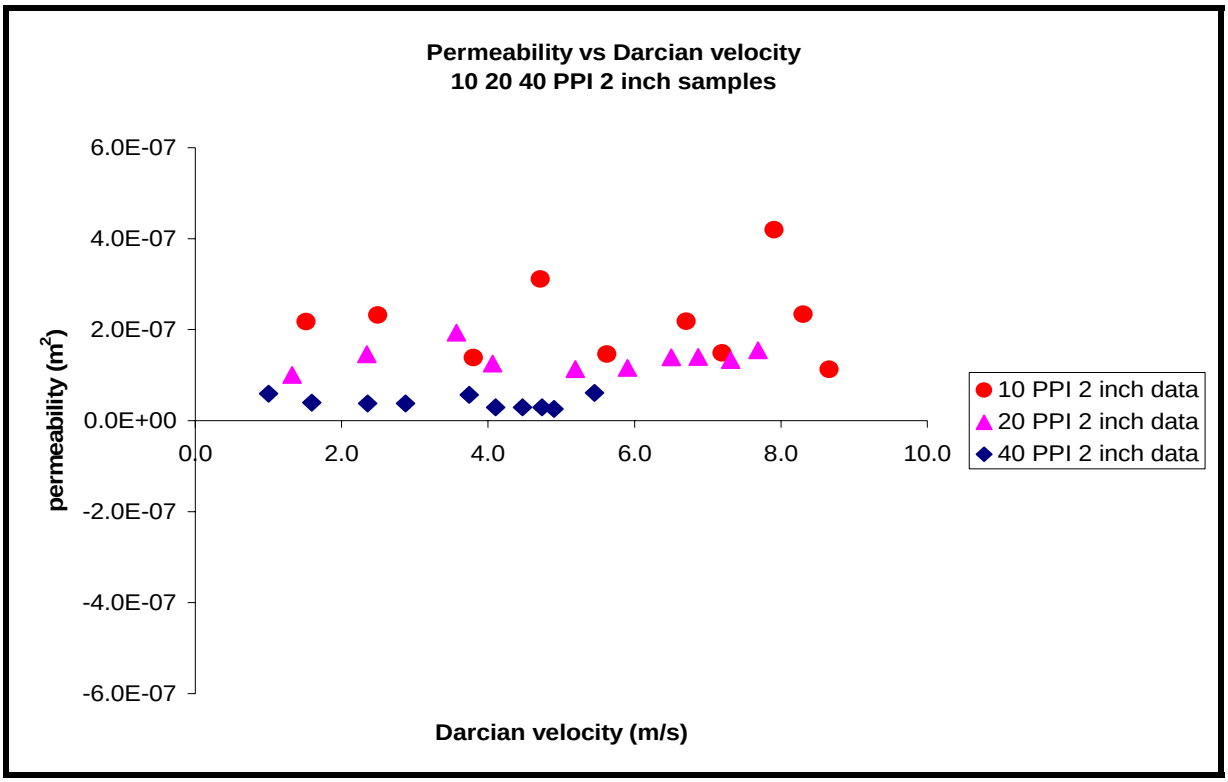

Figure 3.12 Permeability vs Reynolds number for 10, 20 and 40 PPI 2 inch samples with similar porosities.

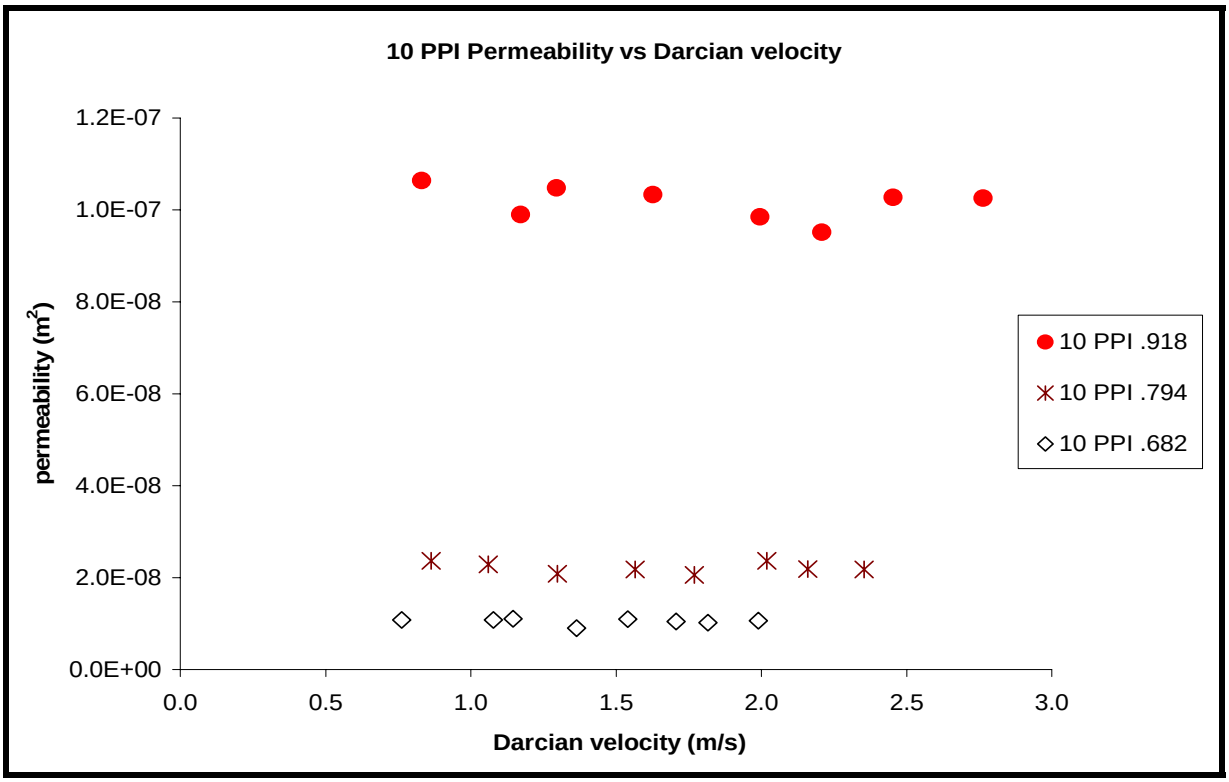

Figure 3.13 Permeability vs Reynolds number for 10 PPI 2 inch samples with different porosities.

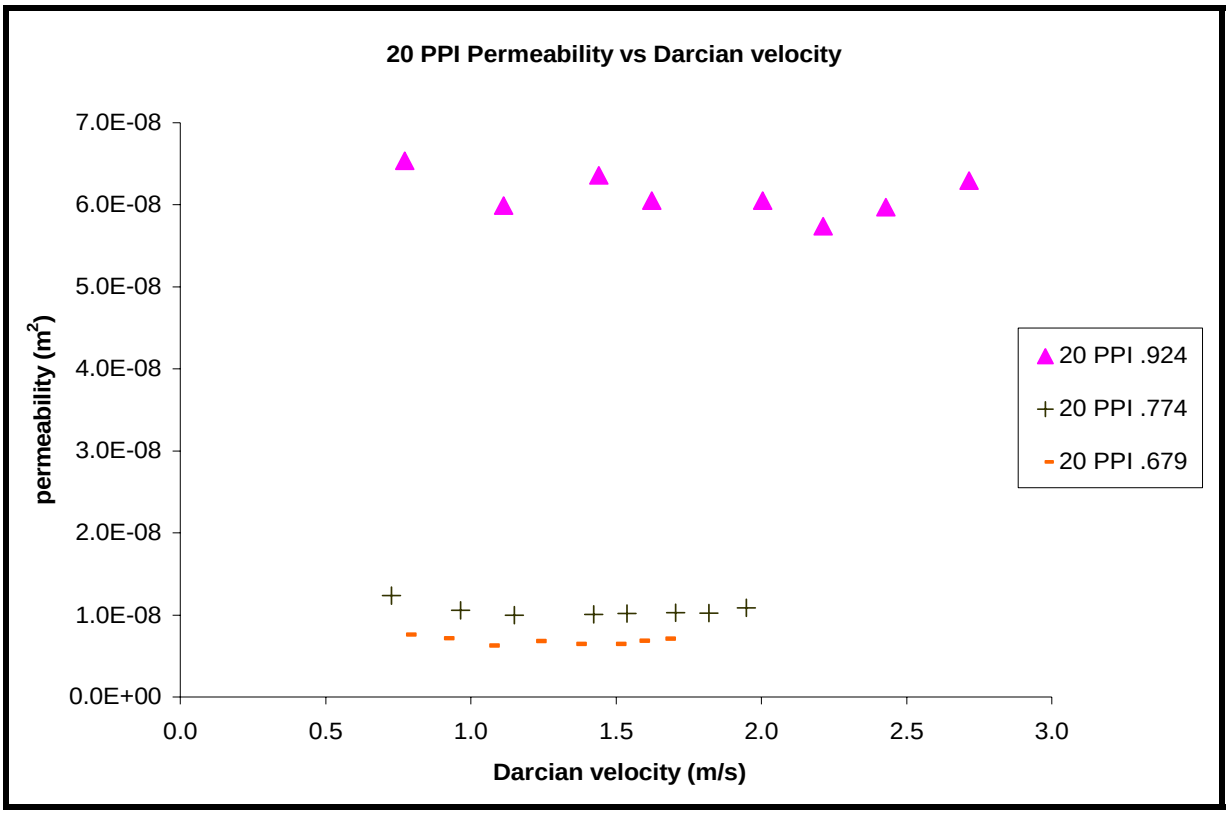

Figure 3.14 Permeability vs Reynolds number for 20 PPI 2 inch samples with different porosities.

Although with some variation in values, Fig. 3.12 through 3.14 shows how as porous density increases and porosity decreases the permeability value increases, decreasing the resistance of the flow through the porous medium. This behavior is consistent with other investigations and the fact that as the porous density increases there is a reduction of cell mean diameters and a greater number of ligaments that obstruct airflow. It should be recognized that the Darcy law is a linear phenomenon applicable for very low Reynolds number (Re << 1), for which there is a slight change in permeability. When the second order regime of Eq. 3.1.2 is reached, especially in the turbulent regime which is the regime experienced in this investigation, variations in the values of the permeability will be evident as shown in Fig. 3.12 through 3.14 and increasing with Reynolds number.

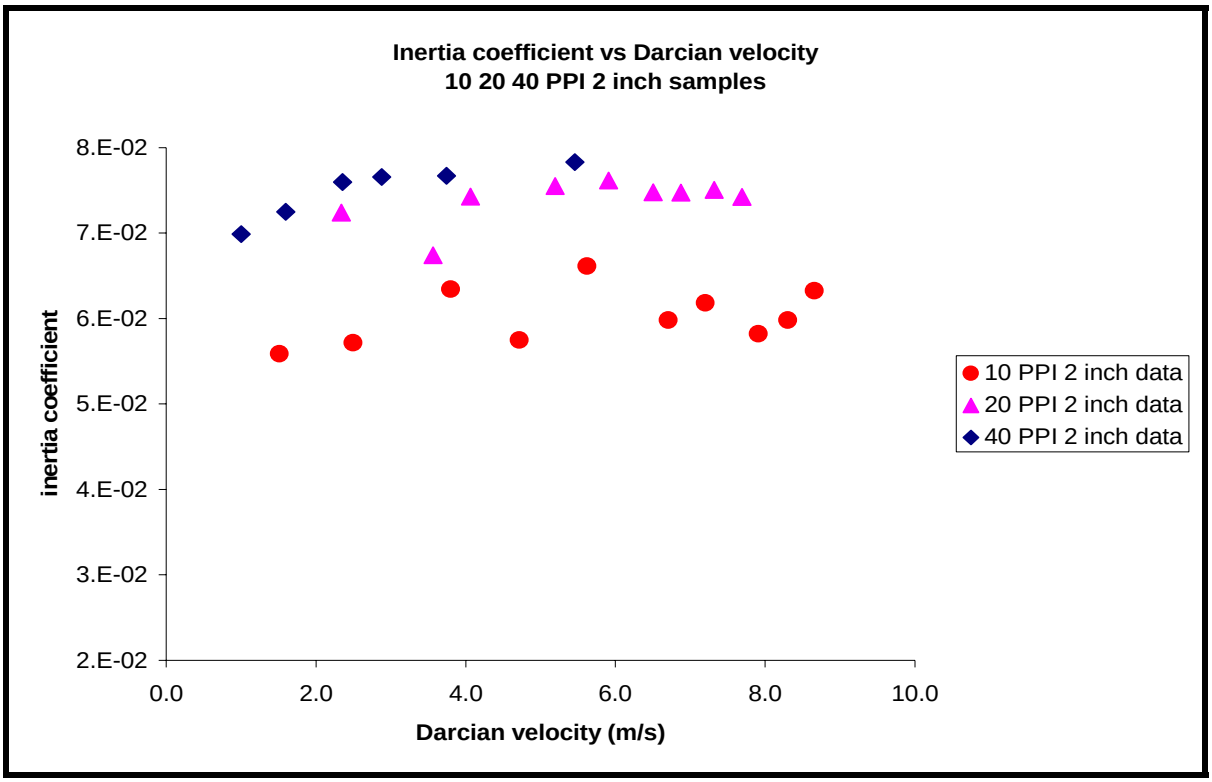

Figure 3.15 Inertia coefficient vs Reynolds number for 10, 20, and 40 PPI 2 inch samples with similar porosities.

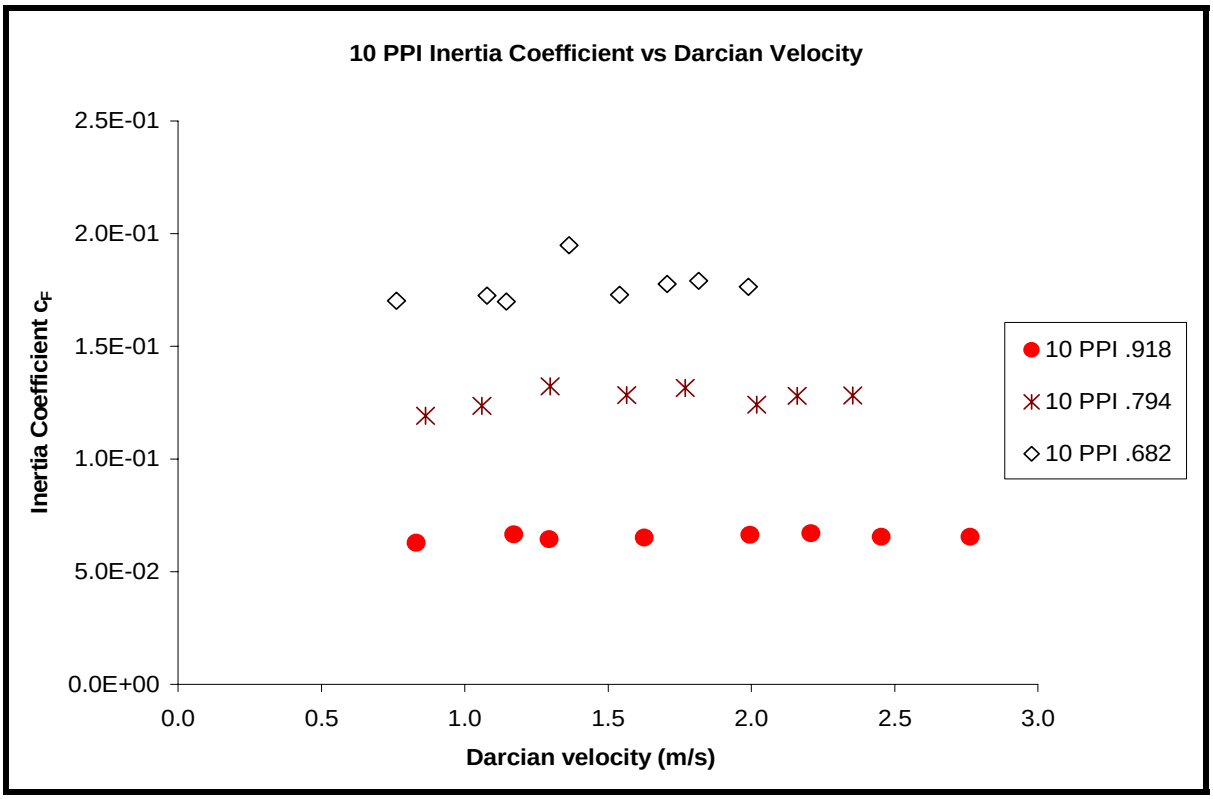

Figure 3.16 Inertia coefficient vs Reynolds number for 10 PPI 2 inch samples with different porosities.

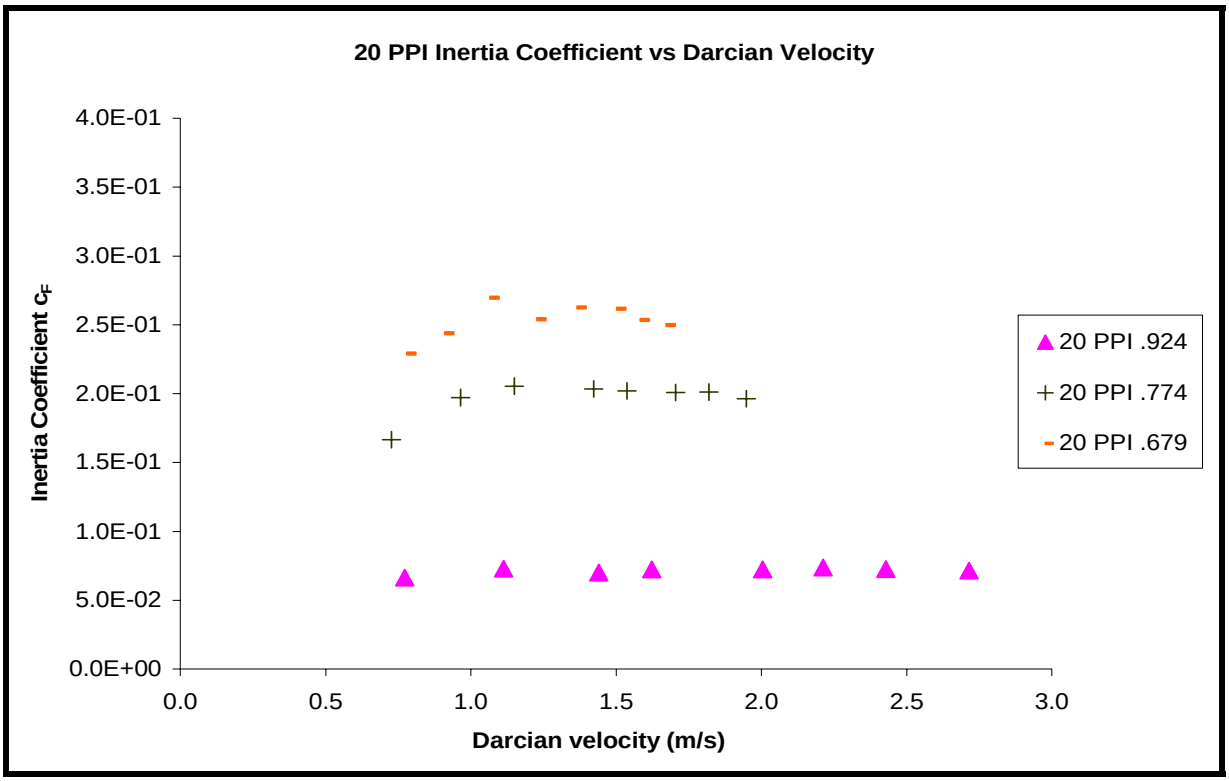

Figure 3.17 Inertia coefficient vs Reynolds number for 20 PPI 2 inch samples with different porosities.

In Fig. 3.15 through 3.17 the variations of the inertia coefficient with Reynolds number its evident showing the increase in the inertia coefficient value as the pore density increases. This results because as the pore density increases there is an increase in material cell filament promoting the increase in drag of the fluid, thus increasing the value of this coefficient. It is proper to mention that at the Reynolds range we are working in the dominant term in Eq. 3.1.2 is the second term which is related to the inertia forces acting on the fluid by the solid structure. This phenomenon arises since at this range the dominant term is the inertia related term at a microscopic level in the porous medium.

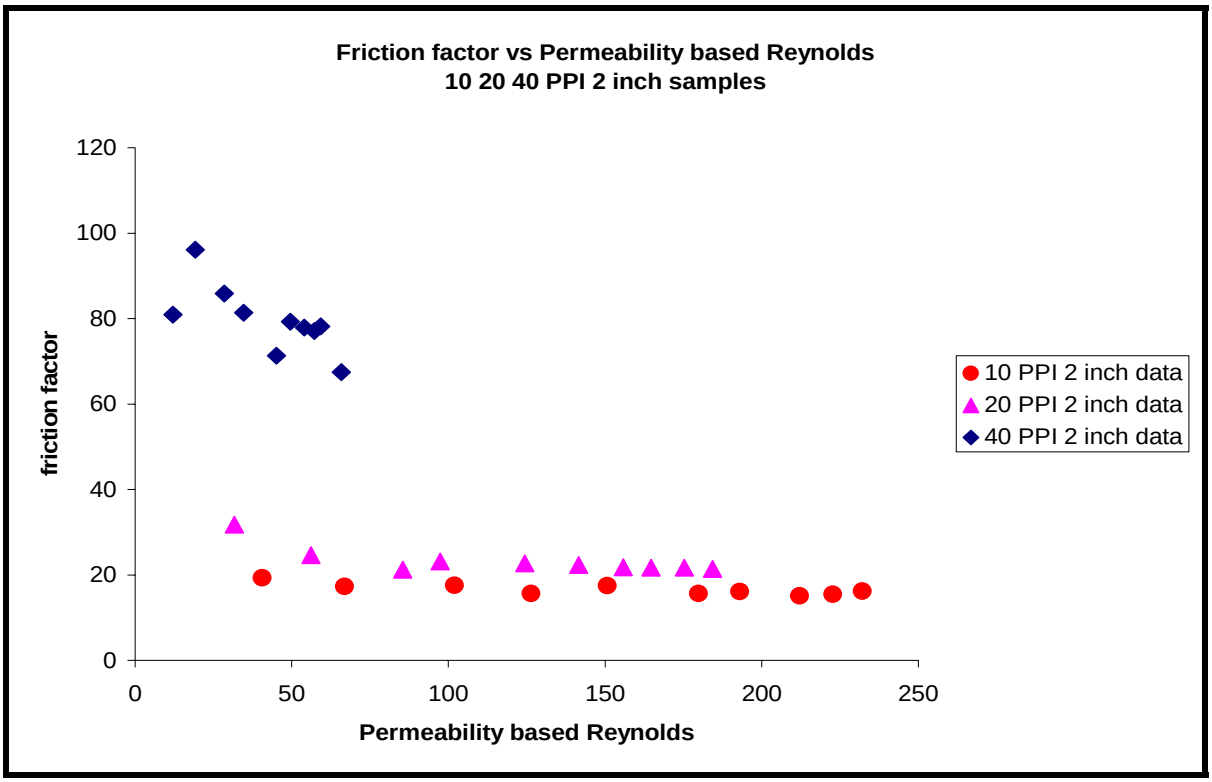

Figure 3.18 Friction factor vs Reynolds number for 10, 20 and 40 PPI samples with similar porosities.

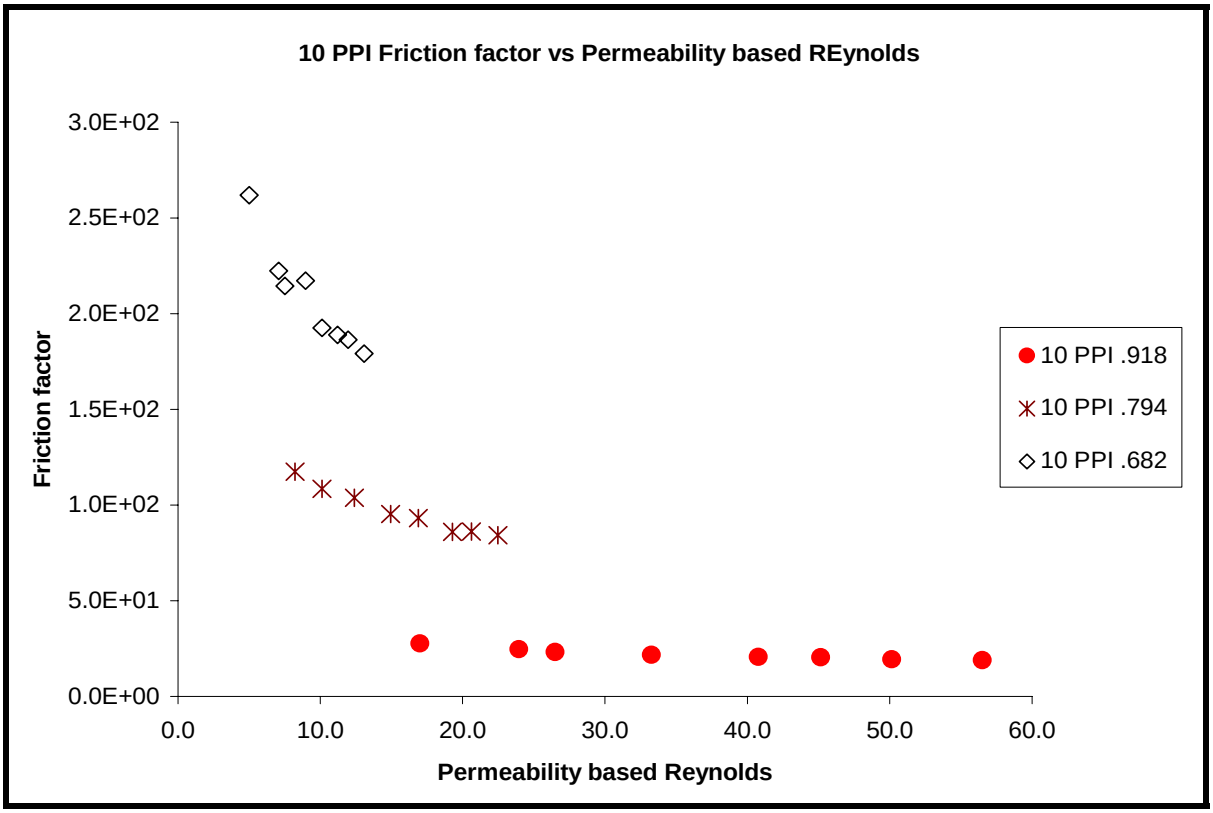

Figure 3.19 Friction factor vs Reynolds number for 10 PPI samples with different porosities.

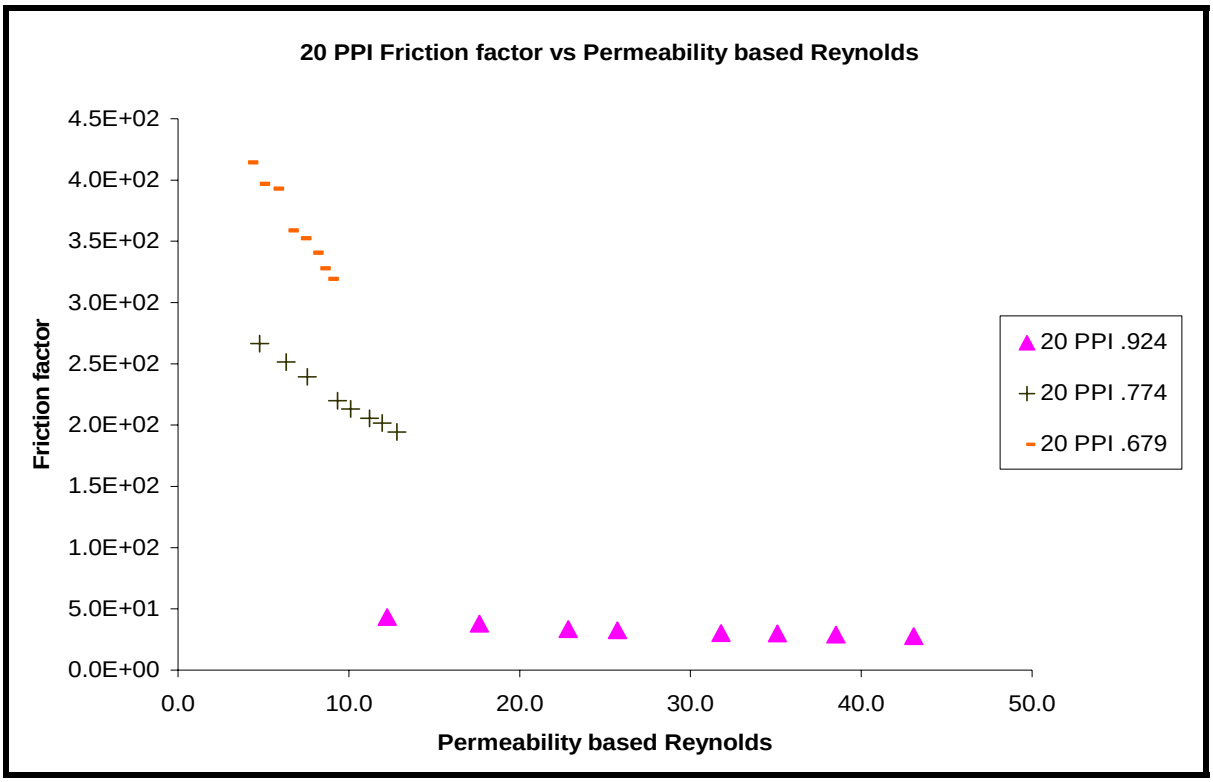

Figure 3.20 Friction factor vs Reynolds number for 10 PPI samples with different porosities.

In agreement with previous studies with flow through high porosity porous media it is observed in Fig. 3.18 through 3.20, the decrease to a practically constant value of friction factor as Reynolds number increases. It is also noticeable that there is an increase in friction as porous density increases and porosity decreases. As mentioned earlier this is consistent with the fact that as the pore density increases the mean pore diameters are reduced and the number of cell ligaments increases per unit area of the sample increasing the pressure drop as the velocity is increased with the reduced void area resulting in a higher friction value.

3.5 Empirical Model

It has already been said that the permeability and inertia coefficient of a fluid while flowing through a porous medium is quantified by the Darcy-Forchheimer equation (Eq. 3.1.2). These flow parameters usually called Darcian (K) and Non-Darcian (c_F) parameters are assumed to incorporate the structural properties of the medium and to be a function of bed characteristics only. Of the correlations that take into account the characteristics of the medium, the one proposed by Ergun (1952) is the most frequently used.

Although this correlation was based on experimental work done with packed beds for which the porosities are lower than the actual metallic foams used, nevertheless a correlation can be obtained based on Ergun's idea.

$$\frac{\Delta P}{L} = 150\frac{(1-\varepsilon)^2}{\varepsilon^3}\frac{\mu v}{{d_p}^2} + 1.75\frac{(1-\varepsilon)}{\varepsilon^3}\frac{\rho v^2}{d_p} \qquad (3.5.1)$$

In this equation ε is the porosity of the beds and d_p is the mean surface volume diameter of the particles.

It is known that the flow parameters are dependent on geometrical factors of the medium and that one of the difficulties dealing with highly porous materials is to determine the structural characteristics of the foams. Various authors have proposed geometrical models and have

scrutinized metal foam geometries but without much success. This is given to the fact that there are a number of manufacturers and different methods of making these materials. For this reason the best way to characterize metal foams still rely on the formulation of empirical models.

In the present literature not much attention has been given to try to correlate metallic porous mediums with a similar method. This is why in this part of the experimental work an Ergun type correlation will be proposed for the samples tested.

$$\frac{\Delta P}{L} = \alpha \left[\frac{(1-\varepsilon)^2}{\varepsilon^3 D} \right]^m \mu v + \left[\frac{(1-\varepsilon)^2}{\varepsilon^3 D} \right]^n \rho v^2 \qquad (3.5.2)$$

In Eq. 3.5.2 α and β are empirical constants to be determined with the experimental data and D is the ratio of the known geometrical parameters of the metal foams which are the ligament diameter and the cell diameter.

Figures 3.21 and 3.22 show the permeability vs the Ergun coefficient, $(1-\varepsilon)^2/\varepsilon^3 D$, and Inertia coefficient vs Ergun Coefficient.

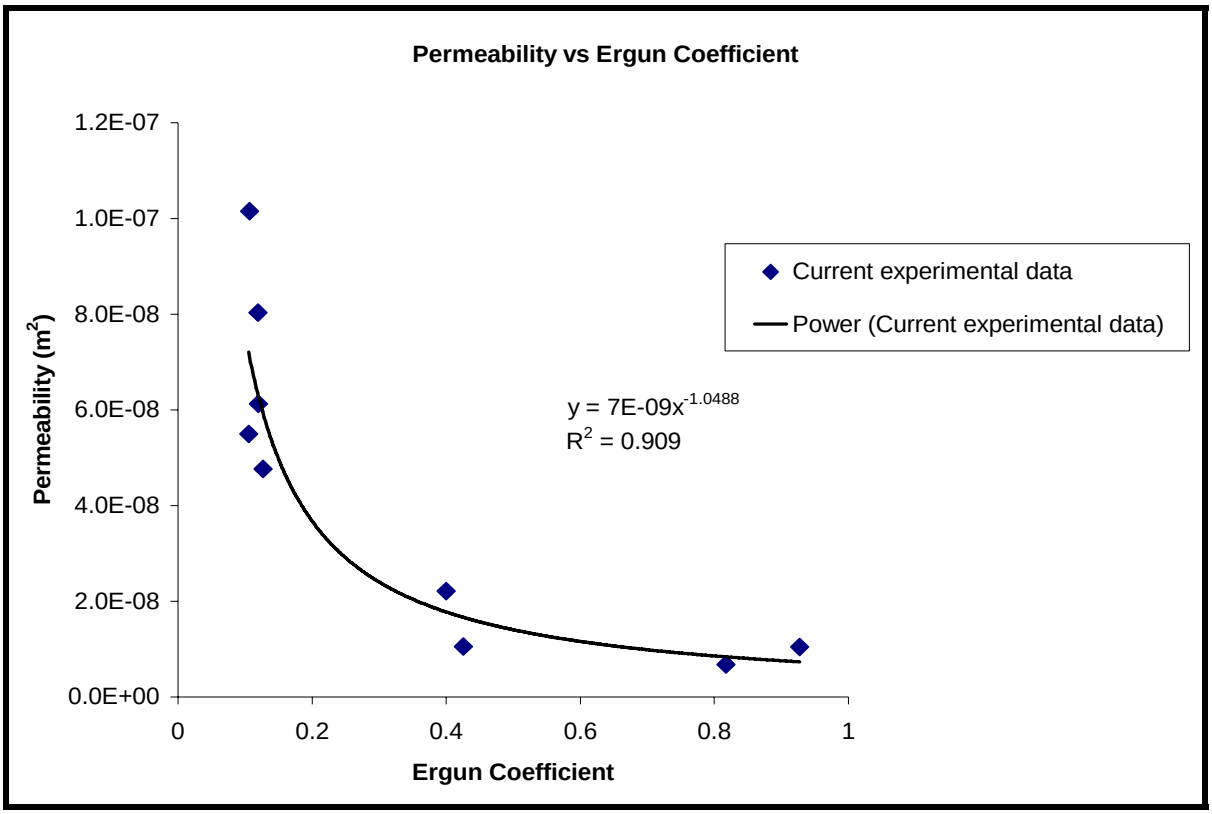

Figure 3.21 Permeability vs Ergun coefficient

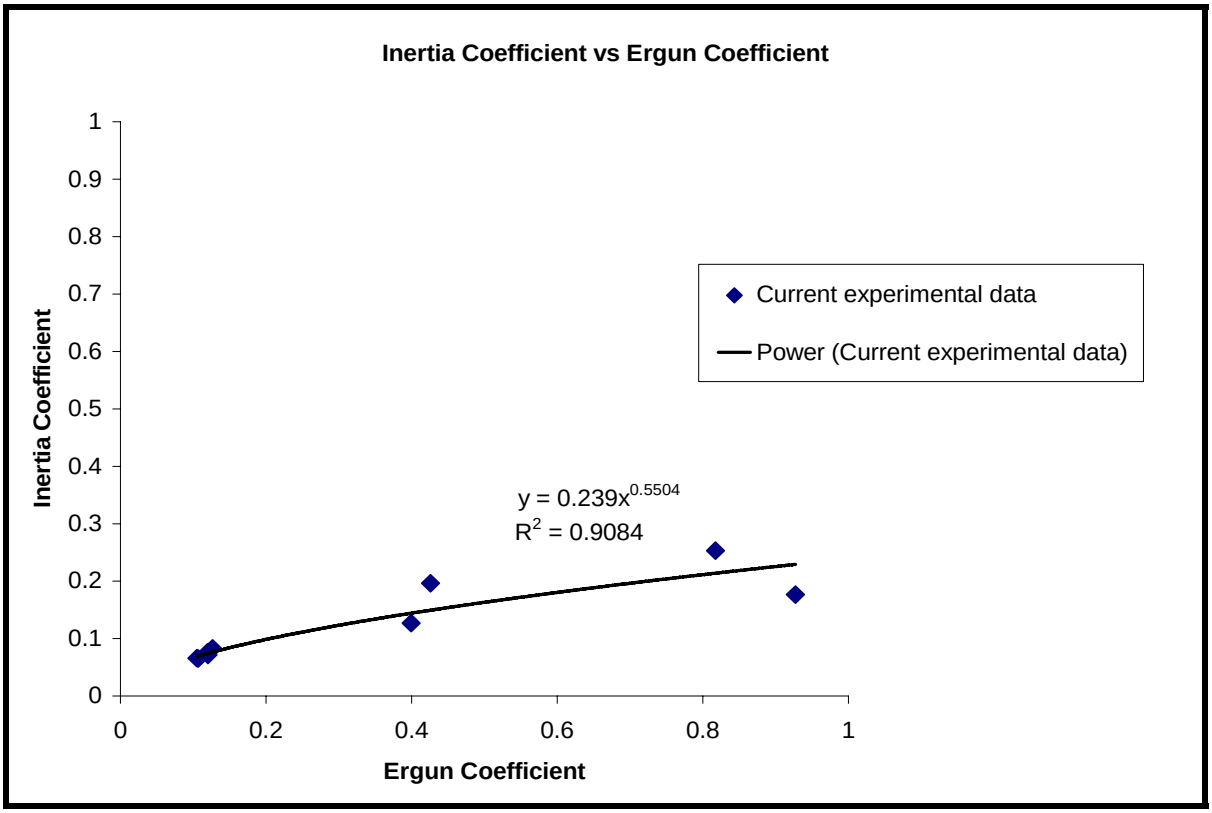

Figure 3.22 Inertia coefficient vs Ergun coefficient

The resulting curve fit of the experimental data yields the following empirical constants, α = 1.4286E+8, β = 2856.60, m = 1.0488 and n = 1.0748.

So the proposed correlation becomes as given in Eq. (3.5.3).

$$\frac{\Delta P}{L} = 1.4286E+8\left[\frac{(1-\varepsilon)^2}{\varepsilon^3 D}\right]^{1.0488}\mu v + 2856.60\left[\frac{(1-\varepsilon)^2}{\varepsilon^3 D}\right]^{1.0748}\rho v^2 \qquad (3.5.3)$$

3.6 Conclusions

Various samples of open cell metal foams were experimentally tested to evaluate their flow characteristics using air as the flowing fluid. Among the samples used there were three different pore densities, 10, 20 and 40 PPI's with a variation of porosities for the 10 and 20 PPI samples. The characterization procedure involved solving the Hazen-Dupuit-Darcy equation for the flow characterizing terms, permeability and inertia coefficient. These two terms accurately describe the pressure drop dependence on fluid velocity and were shown to be applicable to high porosity open cell metal foams.

The following conclusions can be made given the results of this experimental work.

1. Pressure drop increased with decreasing mean pore diameter in the samples with similar porosities and increased with decreasing porosity for the same pore density. This can be attributed to the increase in obstruction in the fluid path as given as the mean pore

diameter and porosity of the sample decrease by means of more solid filaments in the structure or less free flow area.

2. When the mean pore diameter was decreased while the porosity was held constant, this resulted in an increase in flow resistance. This was observed by the reduction of the permeability value and the increase in the inertia coefficient. The same response was obtained when the porosity value decreased in the samples. This increase in inertia coefficient is attributed to the higher specific surface area generated by the smaller pore size

3. As expected the friction factor increased with the reduction of mean pore diameter, which increased the number of cell ligaments per unit area increasing the pressure drop as the velocity is increased with the reduced void area in the medium.

4. For different ranges of Reynolds number or velocity regime the values of permeability and inertia coefficient varied. Then whenever these flow parameters are stated for a high porosity porous medium, the Reynolds range for which these values were calculated must be specified for better accuracy.

5. An Ergun type correlation has been proposed obtained with the experimental data.

CHAPTER 4 Forced Convection in Metal Foams

This chapter will focus on forced convection experimentation in metal foams of various pore densities and porosities. A Nusselt correlation will be given with the experimental data obtained with the various samples tested. The resulting information can be used in the aid of numerical simulations and design of compact heat exchangers and heat sinks.

4.1 Introduction

Porous media has been widely used for many heat transfer application. They can be in the form of packed beds, sintered materials or foam materials. In the past a large amount of research work for packed beds and sintered materials has been done [30,31] and extensive data and empirical correlations for convective heat transfer coefficient are available in the literature for a variety of particle diameters, Reynolds numbers and fluids. But metal foams have not been studied to the same extent [32,33,34,35] and there are no data available for compressed foams in the present literature. Therefore there is still a lot of experimental work to be done with metal foam to provide the sufficient data for the design of thermal systems.

Forced convection through metallic foams has been proved to substantially enhance heat transfer rates. Given this characteristic of the material, metal foams are well suited for the use in high performance compact heat exchangers and heat sinks for the use in electronic equipment and other industrial applications. Among the advantages of this material are the machinability,

availability and low cost, and weight reduction, given its high porosity, compared with other types of materials used for heat dissipation. Convective heat transfer in a fibrous medium involves the formation of complex flow and temperature fields around individual fibers. Flow separation may occur around the fibers at higher velocities than that of creep flow [35]. Even though this leads to higher pressure drop values, the associated mixing substantially enhances the heat transfer rate. In addition when the fluid saturated medium has a larger effective thermal conductivity than the fluid alone, the heat dissipation is enhanced this in turn helps to keep the surface temperature within acceptable limits [6].

When working with heat transfer in porous media two heat transfer coefficients are often calculated to quantify heat transfer characteristics in the medium given the need for the characterization or application. The interstitial heat transfer coefficient describes the heat exchange between the fluid stream and the solid matrix of the porous medium. The second heat transfer coefficient is the wall heat transfer coefficient. This coefficient describes the global heat transfer between the wall surface and the porous medium and is most useful in the design of heat sinks for electronic cooling applications. In this experimental chapter the wall heat transfer coefficient will obtained for various samples of pore density (10, 20, 40 PPI's) and porosities ($0.60 < \varepsilon < 0.93$).

4.2 Equipment

The samples used in this experimental part of this thesis were the same samples used in the fluid flow experiments in Chapter 1 with the same properties as those specified in Table 2.1. Also the same TecQuipment air duct was used with the handheld omega anemometer (Omega HH-30A) attached at the exit of the air duct to measure the average air velocity at the duct. The heaters used in this experimental part were manufactured by Minco, Inc. They are made of Silicone Rubber, which is a rugged, flexible elastomer material with excellent temperature properties (Fig. 4.1). Silicon Rubber heaters are ideal for applications with limitations in space, as in the case of the experimental set-up constructed for this research. The temperature range in which this kind of heaters can work is from -45 to 235°C (-50 to 455°F). The heaters used had the same base size of the samples used (4" X 2"). They have an electric resistance of 331 Ω and the maximum power that this kind of heater can supply is 40 W at 115 VDC. The wires by which the heater is 48 fed have a diameter of 0.050" to support the necessary current for the power mentioned.

Figure 4.4.1 Minco kapton thermofoil heater

A DCS150-8EM1 DC power supply manufactured by Sorensen was employed in the research. This power supply has a 0-150VDC voltage output range and a current range of 0-8

AMP. The maximum output power is then equal to 1200 W. The following components made the data acquisition system used.

- Computer
- SCXI 2000 chassis
- SCXI-1200 module DAQ device
- SCXI 1122 signal conditioning module 50
- SCXI-1322 terminal block
- Serial cable
- 7-inch Parallel-port cable adapter
- Type T thermocouples

The computer used was a commercial PC in which Lab View software from National Instruments was installed. The SCXI-2000 is a rugged, low-noise chassis that can hold up to four SCXI modules. This chassis powers SCXI module handles all timing, trigger, and signal routing between the digitizer and SCXI modules. SCXI-1200 is a device that can be used to acquire data and as a control module. It has eight analog input channels, 24 Lines of TTL-Compatible Digital I/O and 16-Bit counter/timer. The National Instruments SCXI-1122 is designed for a wide variety of sensor and signal inputs requiring isolation. This module can acquire strain, RTD, thermocouple, millivolt, volt, 250 V, 0 to 20 mA, and 4 to 20 mA current input signals. Terminal blocks, as the SCXI 1322, are devices designed for specific input types, such as thermocouples, strain gauges, and high-voltage inputs. SCXI-1322 terminal block is compatible with the SCXI-1122 module. The serial cable is a RS-232 communications cable. The 7-inch parallel port cable

adapter is a small cable with serial ports that was used to connect the SCXI- 2000 chassis to the SCXI-1200 DAQ device. T type thermocouples were used. These thermocouples are made of Copper and Constantan, and they are employed in applications where the temperature is less than 400 ^{o}C.

4.3 Experimental Procedure

The objective of this chapter is to obtain a Nusselt correlation with the experimental data gathered with the aluminum metal foam samples. The set-up used for this section is the same set-up used for the flow experiment (see section 2.3) with some modifications to include the applied heat flux at the base of the samples and the equipment used for the temperature measurements. A schematic of the experimental set up is shown in Fig. 4.2. The same aluminum foam samples that were used in the flow experiments, and as detailed in Table 2.3, were used in the forced convection experiments with the exception of the 40 PPI sample of 4 inches in depth (last sample in Table 2.3).

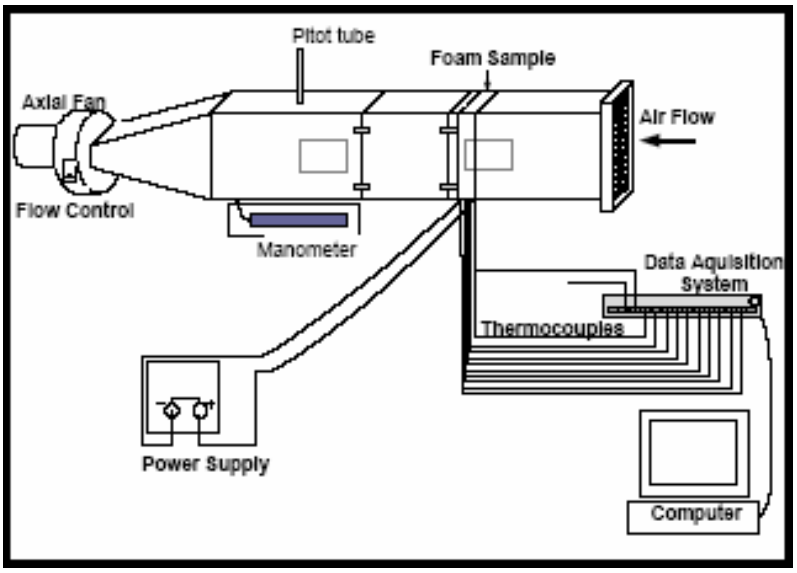

Figure 4.2 Experimental set-up for forced convection experiments

The samples were heated with the Minco Kapton Thermofoil heaters with the same dimensions as the base of the samples (4" X 2"). Three holes were drilled in the base of each sample at distances in the x or flow direction of 0.5, 1 and 1.5 inches in order to measure the base temperature in forced convection as shown in shown in Figure 4.3. The holes were drilled carefully so that all the holes had the same depth of 2 inches. Then type T thermocouples were fitted tightly in these holes. Two additional thermocouples were used to measure the inlet and outlet temperatures near the base in order to obtain information of the fluid temperature change. For some samples additional thermocouples were fixed at Y plane perpendicular to the flow direction in order to assure that isothermal conditions existed in that direction. The thermocouples were placed in such a way to ensure that the beads were in contact with the metal base. Then these were connected to the data acquisition system to obtain the temperature readings.

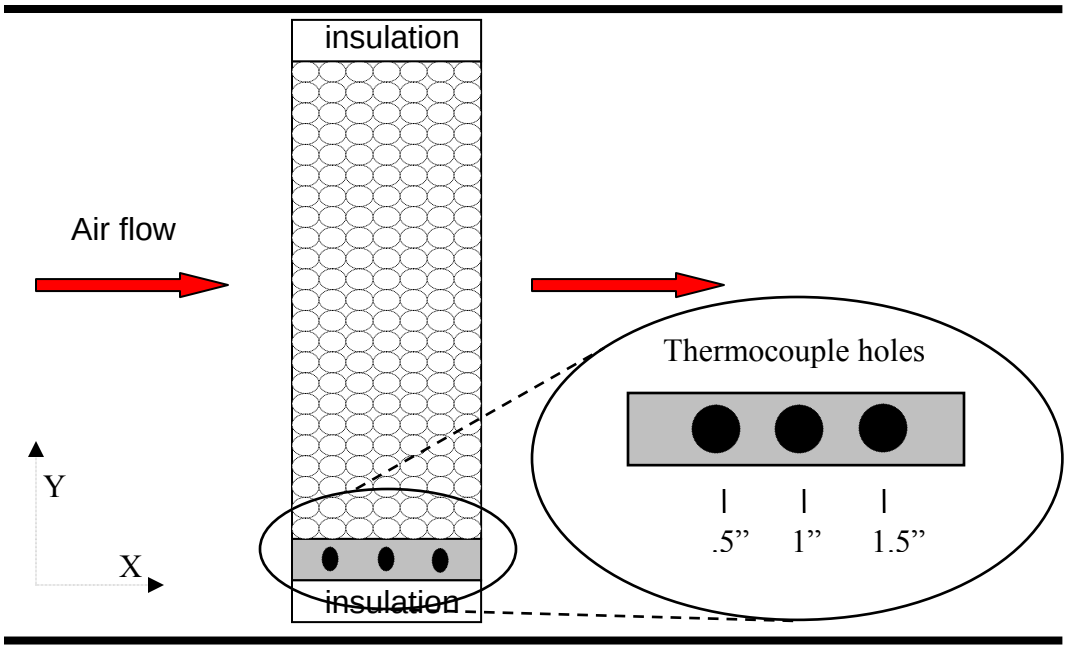

Figure 4.3 Skematic of the side view of the metal foam sample.

The sample was placed in the test section of the air duct after being enclosed in a housing of very low conductivity Styrofoam. This Styrofoam material, which it is easily machined to the desired shape of the sample, offers the advantages of a good insulation thus preventing effectively conduction losses.

Flow measurements were recorded as done in the experimental section of Chapter 3 Section 3, with the only difference that the velocity of the fluid was measured with a hand held anemometer and the average velocity in the duct was calculated using the cross sectional area of the metal foam sample. The average velocity was calculated using conservation of mass as in the second runs of the fluid flow chapter. In this experiment typical velocities ranged from 0.727 to 2.674 m/s.

The Kapton heaters were powered with the power supply to a voltage of 65V. At this power setting the highest fluid temperature difference between the entrance and the exit was less than 20^{o}C, this provided information to ensure that the fluid properties do not change significantly and could be ignored for this experimental work.

Monitoring the values of temperature obtained by the thermocouples during an approximate of 20 minute period of time assured that steady state was reached in the system. Then the temperature readings of the thermocouples were recorded. The isothermal conditions at the plane perpendicular to the flow was verified given that among the samples tested the temperature variation recorded was less than 0.1 ^{0}C.

It is important to clarify that in earlier experimental works of forced convection like Calmidi et al. [32] the effect of varying power input to the heaters was verified. In their experimental work it was found that Nusselt number did not depend on the power input to the heater.

The following graph shows the data gathered for one of the experimental runs made with the 40 PPI sample at different flow velocities of 1.45, 2.10 and 2.25 m/s. It is clear a variation along the axis parallel to the flow direction, increasing the base temperature while we get farther away from the leading edge. This is given because the condition of constant heat flux is obtained at the lower part of the base and the temperature readings are taken at 0.25” from the lower part of the 0.5” base.

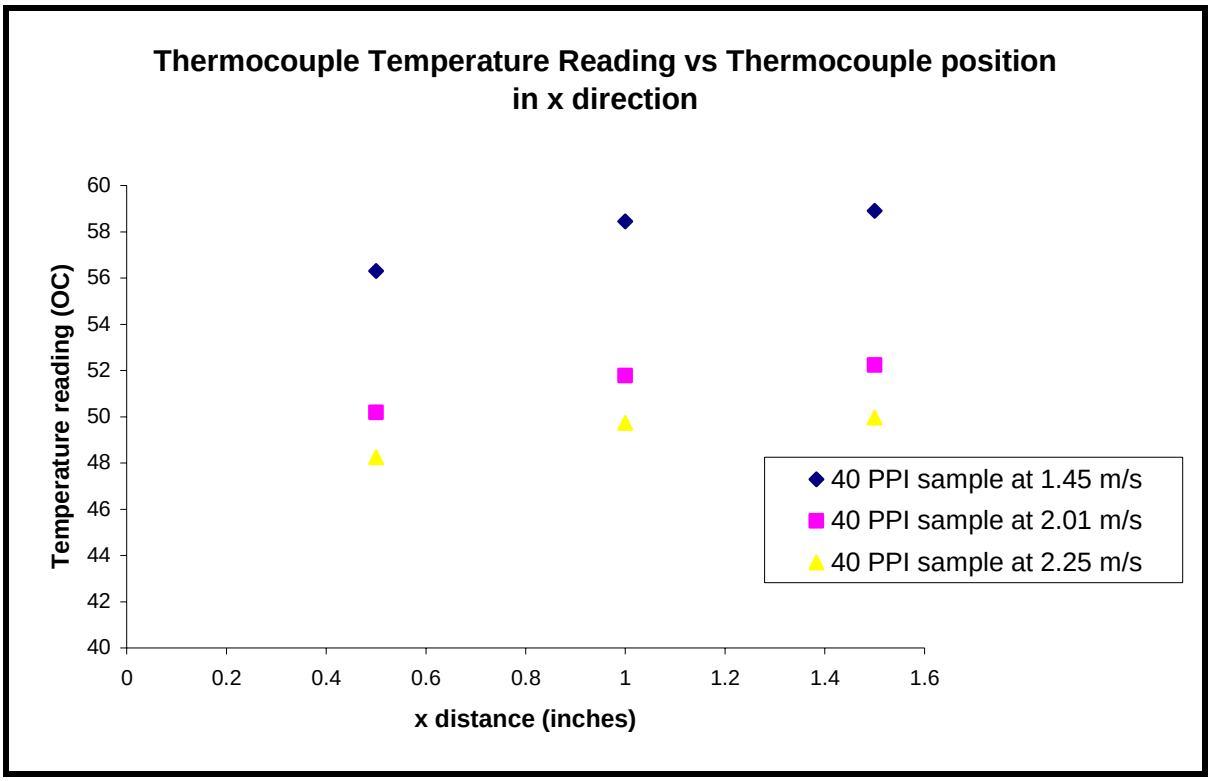

Figure 4.4 Temperature distribution in the x direction for the 40 PPI sample for various velocities.

With the three values of temperatures taken at the base an average is calculated with equation 4.3.1.

$$\Delta T_{avg} = \frac{\sum_{i=1}^{3} T_{base}}{3} - T_{\infty} \qquad (4.3.1)$$

Here T_{∞} is the air temperature at the entrance of the sample. After the Average temperature is obtained the average heat transfer coefficient h, is defined as,

$$\bar{h} = \frac{q}{A\Delta T_{avg}} \tag{4.3.2}$$

Where q is the power input supplied to the heaters and A is the surface area of the metal foam sample. An average Nusselt is calculated using the above information by,

$$\overline{Nu} = \frac{\bar{h}L}{k_e} \tag{4.3.3}$$

Where L is the depth of the metal foam and the k_e is the effective thermal conductivity. There have been numerous studies that predict the effective thermal conductivity for porous media but the issue in estimating the thermal conductivity in metal foams has not been that extensively studied. The analysis of the thermal conduction through a fluid saturated porous medium which calculates the effective thermal conductivity is dependent on the effective local properties of both phases of the medium. When temperatures of the fluid and solid phases remain low, the energy transfer via radiation can be neglected for the thermal conduction analysis leaving only two physical properties of the fluid-saturated system, effective local thermal conductivity (k) and the local heat capacitance (ρc_p). This local heat capacitance can be obtained through volume averaging methods. So three governing factors of the effective thermal conductivity in a fluid-saturated medium are, the thermal conductivity of each of the phases, the structure of the solid phase and contact resistance between particulates in the solid phase, if the solid is not continuous [6]. Although Boomsma and Poulikakos [36], Calmidy and Mahajan [37] have made conduction models with the analysis of different geometries these do not agree with

the rest of the literature and with the different porous media commercially available by different manufacturers. For this experimental work the use of the simplified one-dimensional conduction model in upper bound configuration were the solid fluid phases are in parallel will be used given in Equation (4.3.4).

$$k_e = (1-\varepsilon)k_s + \varepsilon k_f \tag{4.3.4}$$

In Equation (4.3.4), k_s and k_f indicates the solid and fluid phase conductivity respectively.

4.4 Results

In this section the data obtained in the forced convection experiments will be presented and a Nusselt correlation obtained from the experimental results of the compressed and uncompressed samples will be obtained.

In Fig. 4.5 shows the convection coefficient for the 10 PPI samples with different porosities. It is observed that at a given flow rate or air velocity the value of the convection coefficient increases with decreasing porosity. With similar results in Fig 4.6, the tests done to the 20 PPI samples showed an increase in heat transfer coefficient with a decrease in porosity.

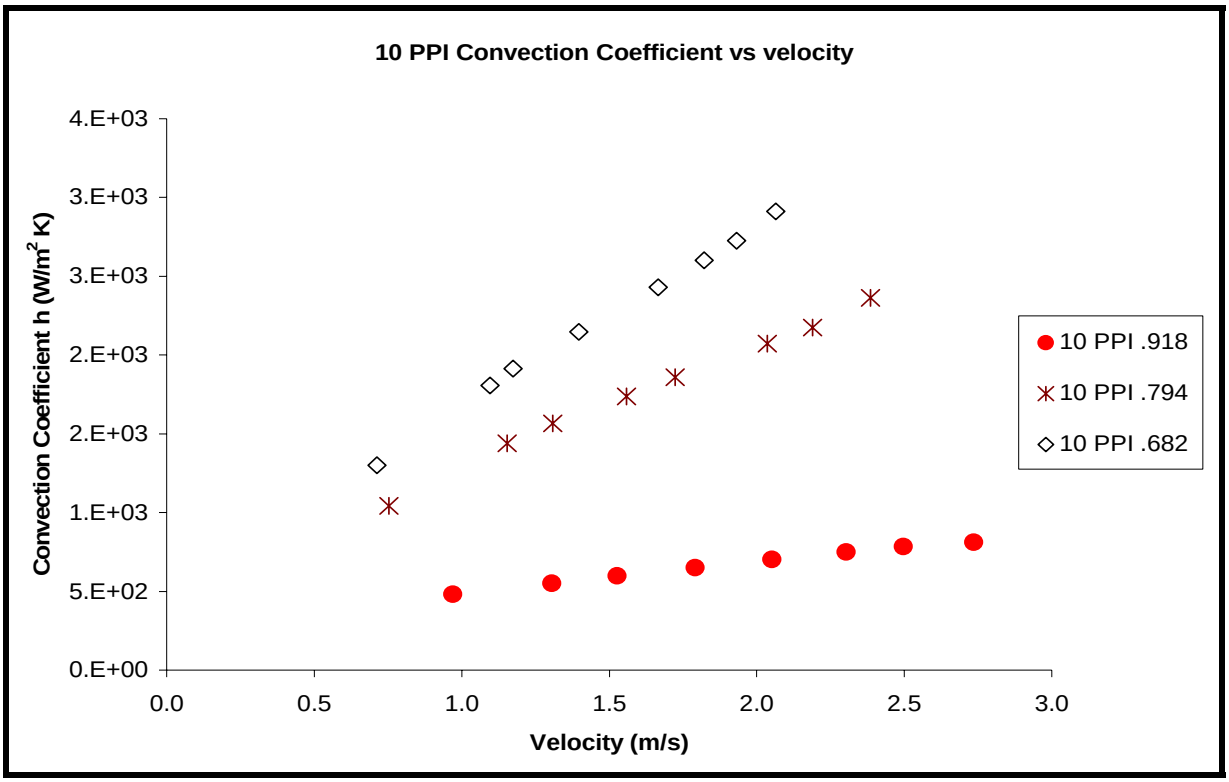

Figure 4.5 Convection coefficient vs velocity for the 10 PPI samples

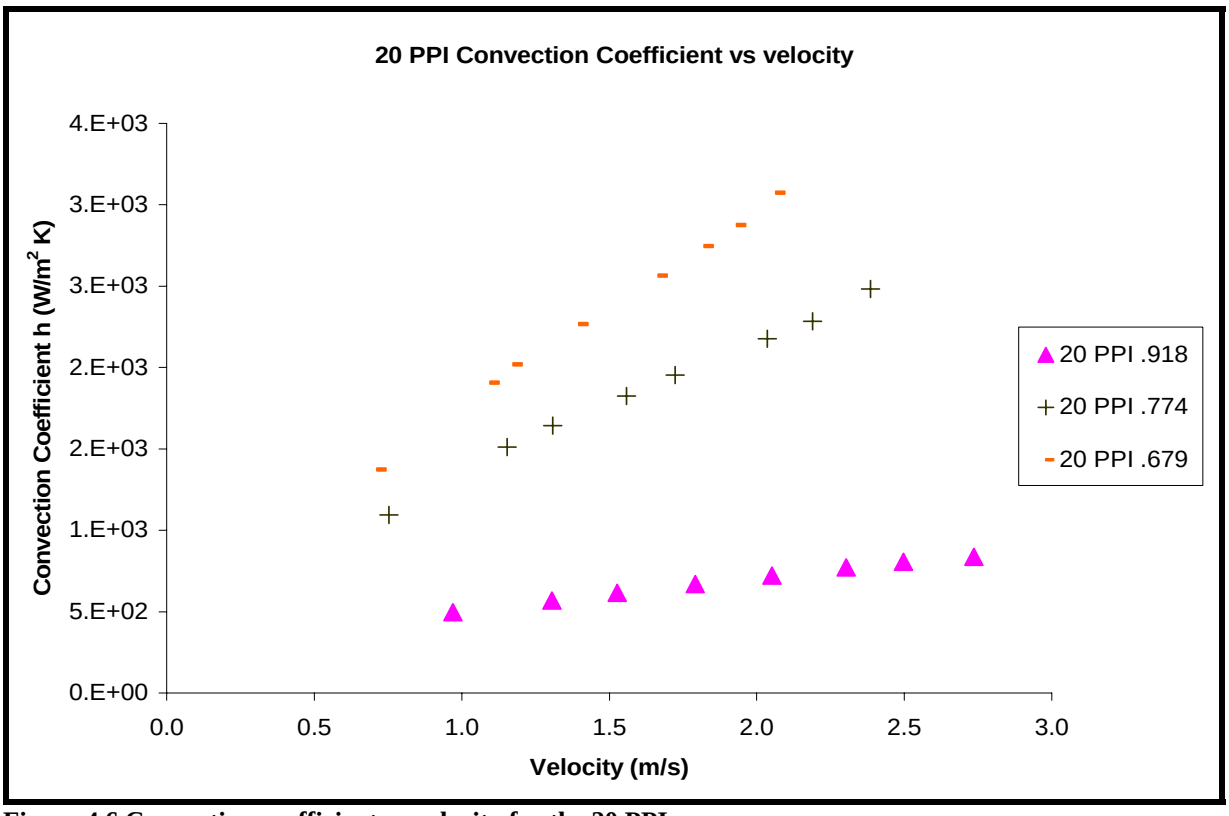

Figure 4.6 Convection coefficient vs velocity for the 20 PPI

With the above results and following Equation 4.4.1, the Nusselt correlation was obtained for the samples used in this experimental section. This Nusselt correlation was correlated following a power law and the results of the empirical coefficients found are described in Table 4.1.

$$Nu = C\,\mathrm{Re}^{r} \tag{4.4.1}$$

Table 4-1 Empirical coefficients

PPI	ε	C	r
10	.918	0.2747	0.5176
10	.794	0.3079	0.6877
10	.682	0.3049	0.7414
20	.918	0.3651	0.5176
20	.774	0.3809	0.6877
20	.679	0.3740	0.7414

4.5 Conclusions

In order to study forced convection in metal foams an experiment was designed to measure the wall heat transfer coefficient in various samples of metal foams with different porosities and pore densities. This was done using air as the working fluid. Analyzing the results in this experimental section the following conclusions were obtained. It is worth mentioning that no earlier works have used compressed samples of various pore densities for the wall heat transfer coefficient.

1. For the uncompressed samples, results have shown that there is a slight increment of heat transfer with the increase of pore density. The value of the convection coefficient is slightly greater for the 20 PPI samples for a given porosity and flow rate. This is given to the fact that turbulence might be promoted with an increase in filament material which would have an enhancement effect in the convection coefficient. Also the increase in effective surface area would be an enhancing factor in the global heat transfer. This enhancement is not as noticeable as for the compressed samples where the porosity is lowered.

2. For the compressed samples the results obtained showed that the porosity of the sample enhances the bulk heat transfer with a decreasing value. It could be observed how the heat transfer coefficient increases with decreasing porosity in both the 10 and 20 PPI samples. This is given to the fact that there is more effective are for conduction transfer enhancing this way the global wall heat transfer.

CHAPTER 5 Thermal Management using Metal Foams

5.1 Introduction

Thermal management, with the increasing and progressive miniaturization of electronic components, becomes a very important aspect and task for engineers designing electronic cooling systems. This large scale integration of electronic circuits has resulted in a continuous increase in chip power dissipation requirements. It is estimated that a power dissipation requirement in the order of 30-50 W/cm^2 is anticipated for the next 5 years resulting in the need for the arrival of new techniques for the use in thermal application that would be affordable and efficient. Forced air cooling has been the preferred cooling technique in electronic equipment, given its simplicity and reliability. Requirements of permissible acoustic noise for electronic cooling restrict the use of mean air velocities above 5 m/s for many applications. Many researchers have studied various solutions to the problem such as vortex promoters and staggered chip arrangements using traditional heat sink technology obtaining 20 to 50 percent improvement; however this will still not be sufficient for the above mentioned upsurge in power dissipation requirement for years to come.

It is known that an increase in a heat sink or heat exchangers exposed area is one of the solutions to obtain an increase in heat transfer, but this will come with a set back to an increase in the pressure drop of the cooling fluid passing through the heat exchanger. An increase in fin density in traditional heat sink technology offers this increase in heat transfer area as some

researchers have already experimented with and even though the arrangement could be a ducted arrangement with free flow area this is not nearly enough for the mentioned heat dissipation requirements. This increase in heat transfer can be managed by more pressure capacity of the fan being used in addition to the ducted arrangements, but still increasing fin densities will increase the weight of the heat dissipation system.

It is one of the objectives in this thesis work to validate what some researchers have already proposed, the use of metal foams for heat exchanger applications. Experimental data will be provided to compare the advantages in weight reduction, increase in heat dissipation capacity and reliability of these materials with a direct comparison to actually available heat sink data for various fin densities. Metal foams provide extended surface area, up to a 10 fold compared with commercially available heat sinks and, although the structure gives an increase in pressure drop as observed in the previous chapter of this work, most of all provides an enhanced heat transfer coefficient due to local thermal dispersion caused by eddies that are shed in the wake of the flow past the medium fibers. It is needless to say that as has been proven in earlier works as that of Cruz [38], the penalty of producing a slightly greater pressure drop could be traded by the enhancement of heat transfer and the reduction in weight that these highly porous mediums offer. This in contrast to traditional heat sinks as is the case for electronic cooling were the system area necessary to provide a same amount of heat dissipation is greater for a given heat flux.

Lau and Mahajan [39] did experimental work with longitudinal heat sinks in ducted arrangements for various fin densities and tip clearances. Their work was focused on providing

useful experimental information for packaging engineers to increase heat dissipation efficiency. In this work they showed that using an appropriate hydraulic diameter, the use of the theories of pipe flow and extended surfaces could be combined to obtain the net heat transfer rates, pressure drop and friction factor information. An important thermal characteristic for designers is the temperature rise for each unit of power dissipation or convective thermal resistance (Θ) Eq. 5.1.1. In any design the designers focus is to keep the thermal resistance to a minimum which revolves basically around increasing the convection coefficient for the system.

$$\Theta \equiv \frac{T_{air} - T_b}{Q} \tag{5.1.1}$$

The heat transfer coefficient (h) represents the amount of heat transferred from the base of the heat sink to the fluid per unit temperature difference and unit effective area Eq. 5.1.2.

$$h = \frac{Q}{(T_b - T_\infty) A_{eff}} \tag{5.1.2}$$

In Eq. (5.1.2.) the effective area depends on both the geometry and conductivity of the fins. For a heat sink the effective area is

$$A_{eff} = A_{base} + n\eta A_{fin} \tag{5.1.3}$$

Where A_{base} and A_{fin} are the base area between two fins and the surface area of the fin respectively and n is the number of fins. The fin efficiency (η) is the ratio of the actual amount

of heat conducted from a fin to that of the ideal amount conducted from a fin at the base temperature. The analytical solution of the fin efficiency for one dimensional conduction in rectangular fins with adiabatic tips can be obtained from any heat transfer text [40] to be:

$$\eta = \frac{\tanh(\lambda H)}{\lambda H} \tag{5.1.4}$$

Where

$$\lambda = \left(\frac{N(L+t)h}{Ltk_s} \right)^{1/2} \tag{5.1.5}$$

Where k is the thermal conductivity of the fin material and N is the number of heating sides of a fin which in general is N = 2. For rectangular fins the effective area is easily calculated as;

$$A_{eff} = nL[S + \eta(2H)] \tag{5.1.6}$$

For generality of the experimental work the known Nusselt, Reynolds and friction factor numbers are used as found in the theory of internal flows in any heat transfer text with the use of hydraulic diameter to take in to account the geometry of the heat sinks. But as previous experimental work it was found that it did not correlate well with the experimental data. Lau and Mahajan [39] in their experimental work found that by modifying the hydraulic diameter the experimental data would correlate well with the theoretical one. A modification of the hydraulic

diameter was made taking into account that the heat sinks where in an adiabatic channel and that the upper part of the heat sink did not contribute to the heat transfer. A heating diameter for the heat sinks was proposed Eq (5.1.7).

$$D_h = \frac{4A_c}{P_h} \tag{5.1.7}$$

Where the heating perimeter represents the peripheral heating area Eq (5.1.8.).

$$P_h = S + 2H \tag{5.1.8}$$

With this characteristic diameter then the Nusselt and Reynolds number become;

$$Nu_h = \frac{hD_h}{k_f} \tag{5.1.9}$$

$$\mathrm{Re}_h = \frac{\rho u D_h}{\mu} \tag{5.1.10}$$

The Nusselt correlation found to fit the experimental data is;

$$Nu_h = 1.42(.023\,\mathrm{Re}_h^{\,0.8}\,\mathrm{Pr}^{0.4}) \tag{5.1.11}$$

To obtain the friction factor and pressure drop the Petukhov correlations [46] and theory of internal flow through pipes were once again used.

$$f = (0.790 \ln \mathrm{Re}_h - 1.64)^{-2} \tag{5.1.12}$$

$$\Delta P = \frac{f \rho u^2 L}{2 D_h} \tag{5.1.13}$$

5.2 Equipment

For this part of the experimental work three smaller samples of metal foams were used as depicted in Figs. 5.1 and 5.2. The purpose of this was to better simulate the dimensions of metal foam heat sinks and the corresponding velocity range for electronic cooling applications.

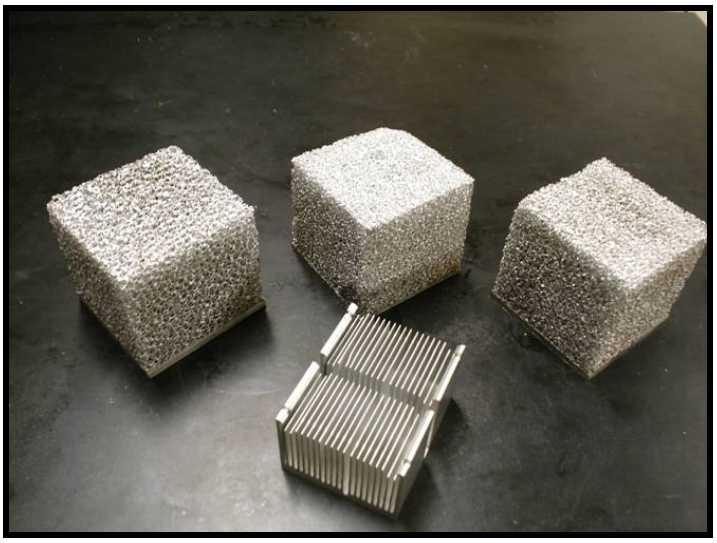

Figure 5.1 Metal foam samples for heat sink applications

The three samples used had cube dimensions (3 in x 3 in x 3 in) for which the height dimensions included a ¼ in aluminum base. The samples had different pore densities (10, 20 and 40 PPI) and the properties detailed in Table 2.2.

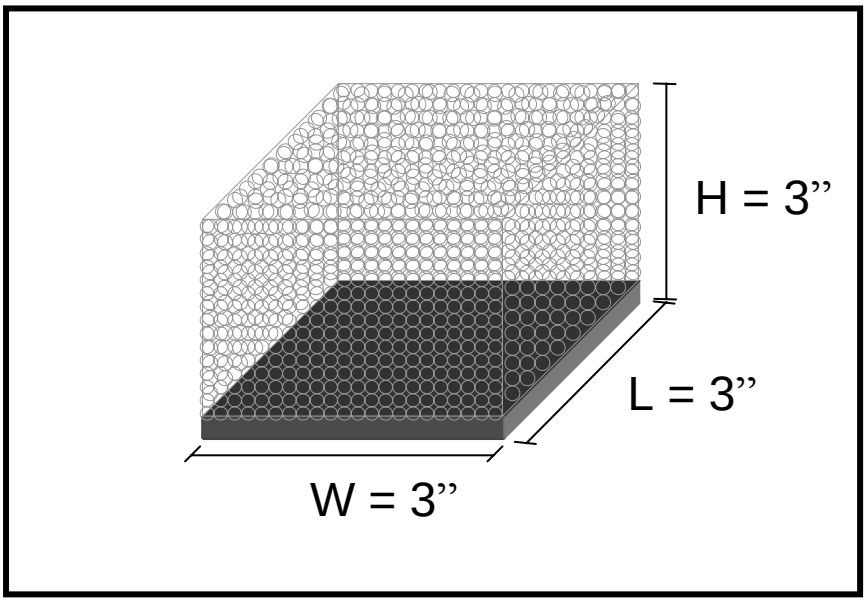

Figure 5.2 Dimensions of the metal foam heat sinks

Table 5-1 Heat sink metal foam properties

PPI	ε	d_L (mm)	d_p (mm)	σ (m^2/m^3)
10	.927	.406	5.080	899
20	.927	.203	2.9	1266
40	.921	.102	1.702	1447

For this part of the experimental work, an air duct was manufactured in the Porous Media Laboratory. A schematic of the wind tunnel is shown in Fig. 5.3. The air duct was built with lexan with a cross-sectional dimension of 3 in by 3 in and a length of 88 in. It has four main parts;

1. The fan assembly
2. The flow straightening area
3. The test section
4. Anemometer section

The fan assembly was made by connecting five 24V muffin fans in series. The flow straightening area was made by making a honey comb of plastic straws and attaching it 1.5 in from the entrance. At the end of the air duct the Omega hand held anemometer reads the fluid velocity at various voltage intervals applied at the fan assembly achieving various air velocities in the experiment. Pressure drop measurements are taken by an inclined anemometer connected to two pressure ports located at 1.5 inches before and after the sample.

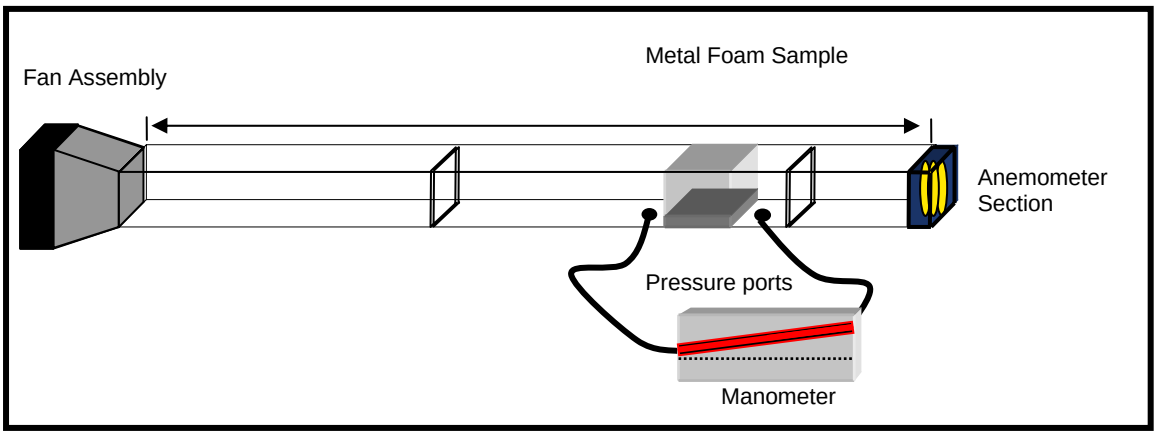

Figure 5.3 Schematic of air duct used for heat sink metal foams experiments

In addition to this the same data acquisition system and power supply described in section 3.2 were used for this experiment. The Kapton Flexible heaters used were manufactured by Omega, model KHLV of dimension 1.5 in X 0.5. A total of 12 heaters were used to cover the entire base of the samples.

5.3 Experiment

One of the primary reasons of this section is to provide a broader view of the heat transfer enhancement of metal foams and possible application in electronic cooling. Although the use of highly porous media in this kind of application may have some set-backs, it will be demonstrated that in general and for certain applications it could be used for thermal improvement.

As a first step toward this demonstration the pressure drop behavior of the samples mentioned in the previous section was studied in an air duct. Afterwards the wall heat transfer coefficient was obtained following the same procedure as in section 3.3. The results of both pressure drop and heat transfer experiments were compared with two of the best commercially available heat sinks with similar dimension to demonstrate both the advantages in thermal resistance and disadvantages of pressure drop increment with the use of highly porous media.

In the second part of this section, using already available longitudinal fin correlations [39] and theory of extended surfaces and internal flow a comparison of longitudinal fined heat sinks vs metal foam heat sinks of the same dimension are evaluated with some promising results.

Finally a weight reduction analysis is made when metal foams are used as heat sinks. This analysis uses a thermal model made by Dukhan and Picon [41].

5.4 Results

For the pressure drop experimentation using the metal foam heat sinks the following ranges of pressure and velocities were achieved as shown in Table 5.2.

Table 5-2 Pressure and velocity ranges obtained in the experimental runs

Sample	Velocity range (m/s)	Pressure Drop Range (Pa)
10 PPI	.84 to 3.36	5.8 to 64.70
20 PPI	.94 to 3.64	11.76 to 120.01
40 PPI	.83 to 3.10	14.21 to 140.58

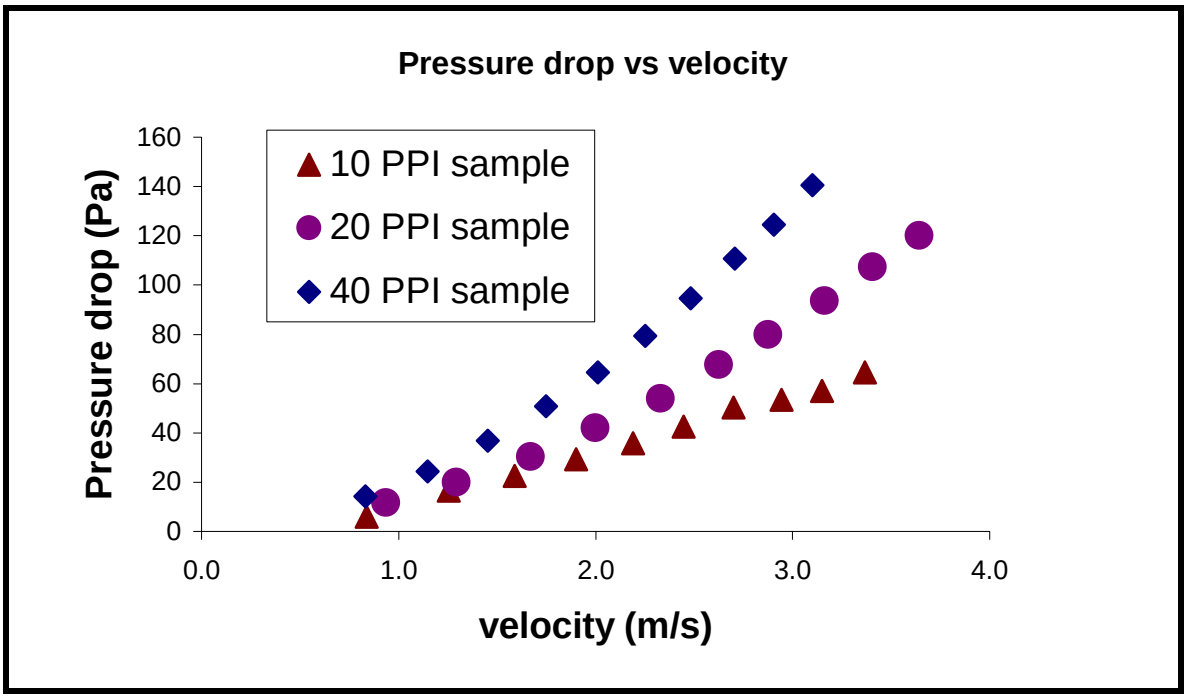

Figure 5.4 Metal foam samples pressure drop vs velocity plot

As expected from the previous section there is an increase in pressure drop as the pore density is increased. This pressure drop will become one of the disadvantages when the comparison to commercially available heat sinks is done. For this section the thermal resistance of the metal foam samples was obtained with Eq. 5.4.1 and the convection coefficient as described in Chapter 4, Eq. 4.3.2.

$$\Theta = \frac{1}{hA} \tag{5.4.1}$$

The following Fig. 5.5 and 5.6 show the results obtained for the thermal resistance and wall convection heat transfer coefficient. These results are in agreement with the results obtained in Chapter 4.

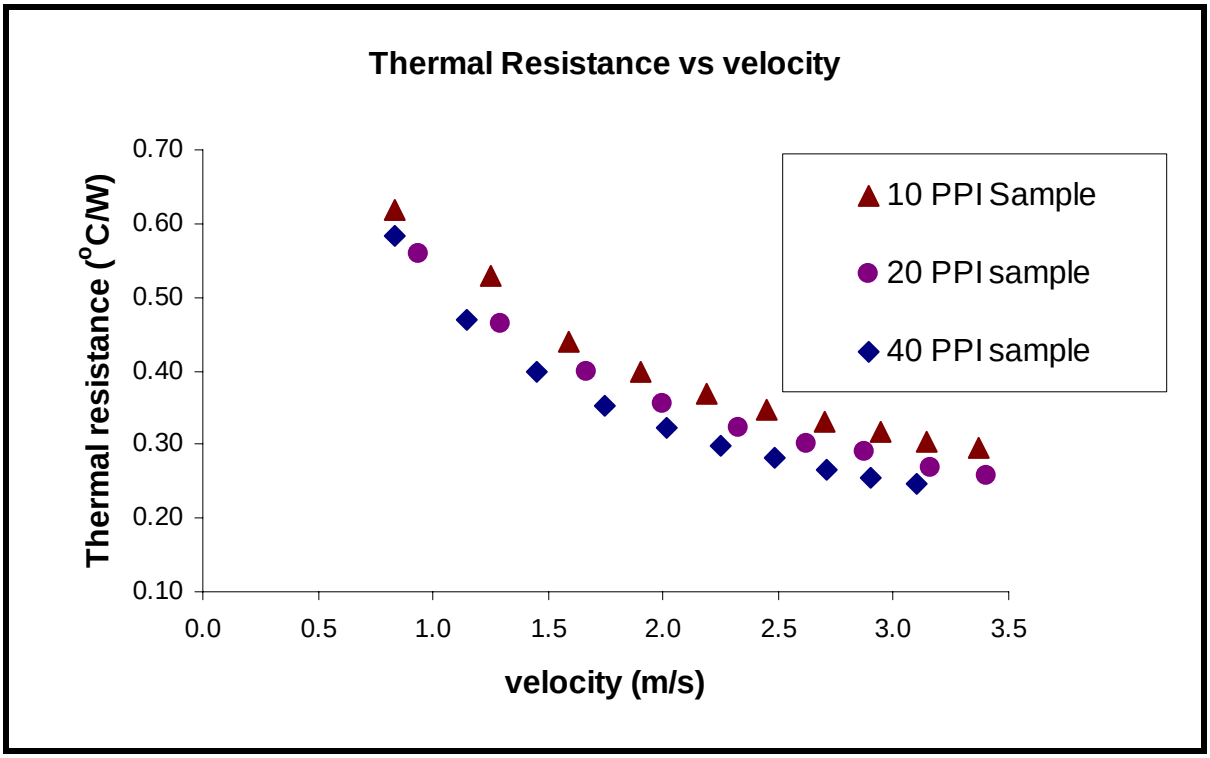

Figure 5.5 Metal foam thermal resistance vs velocity plot

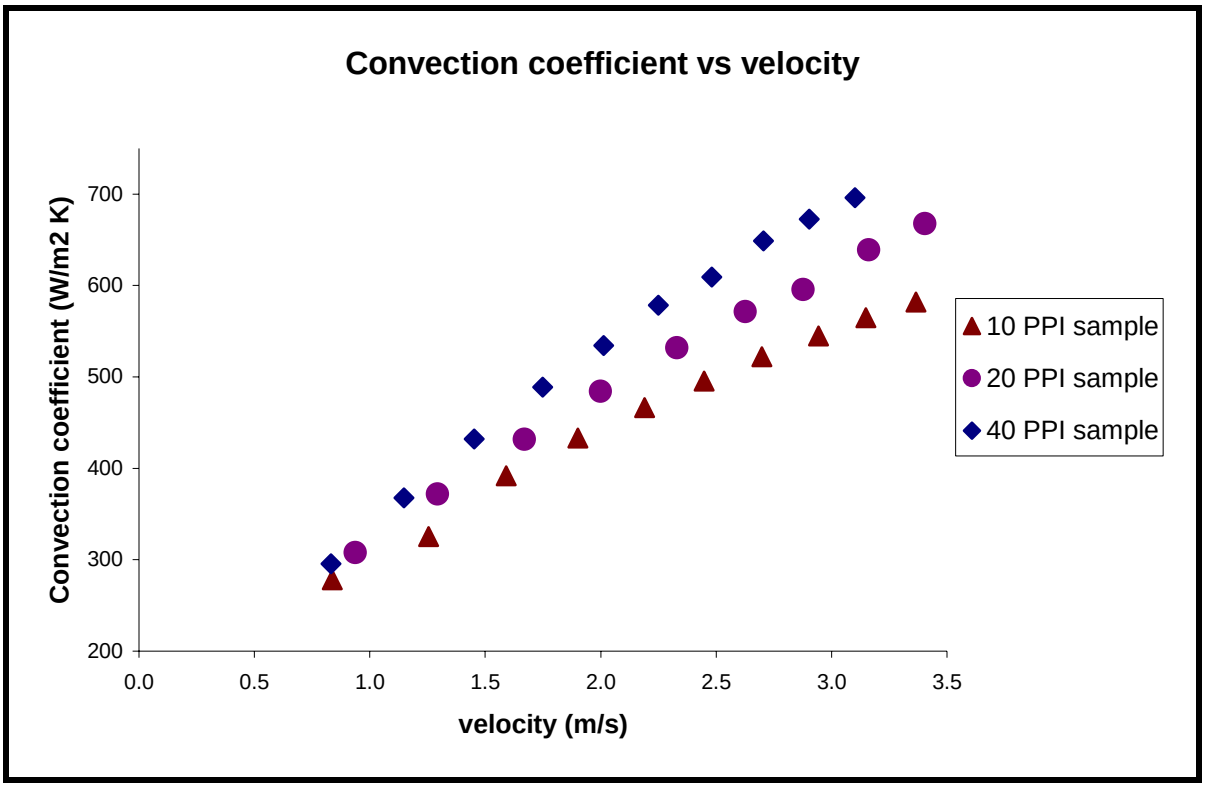

Figure 5.6 Metal foam wall convection coefficient vs velocity plot

Comparison with two of the best commercially available heat sinks is made for the results of pressure drop and thermal resistance. This information is taken from Thermaflo Corporation. Table 5.3 describes the dimensions of the heat sinks and Fig. 5.7 shows the two heat sinks.

Table 5-3 Dimensions of the commercially available and the metal foam heat sinks

Heat Sink (model number)	Width (in)	Length (in)	Height (in)
P817151B00002	3.20	2.80	2.01
P696637B00002	2.7	2.6	1.5
Metal foam blocks	3	3	3

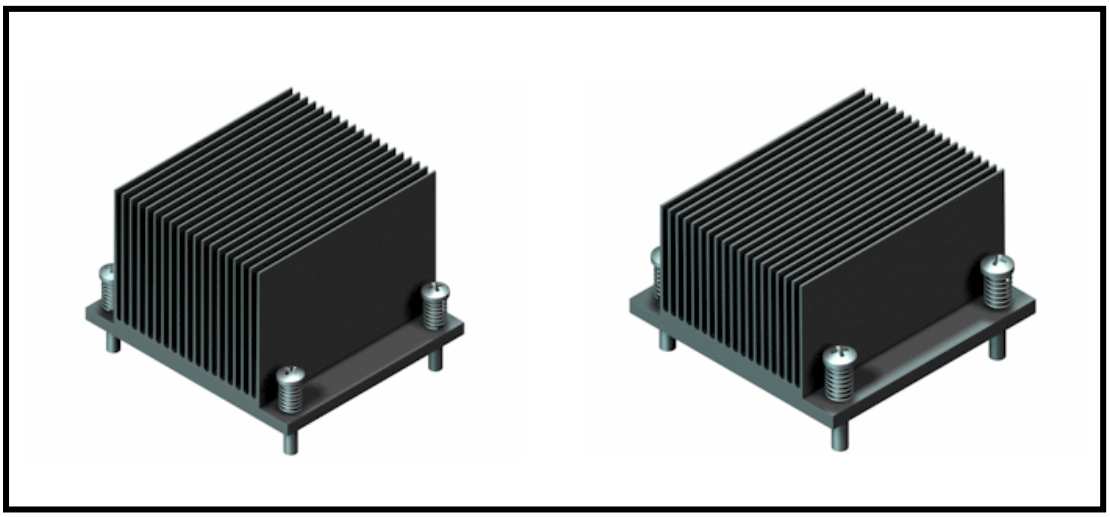

Figure 5.7 Commercially available heat sinks

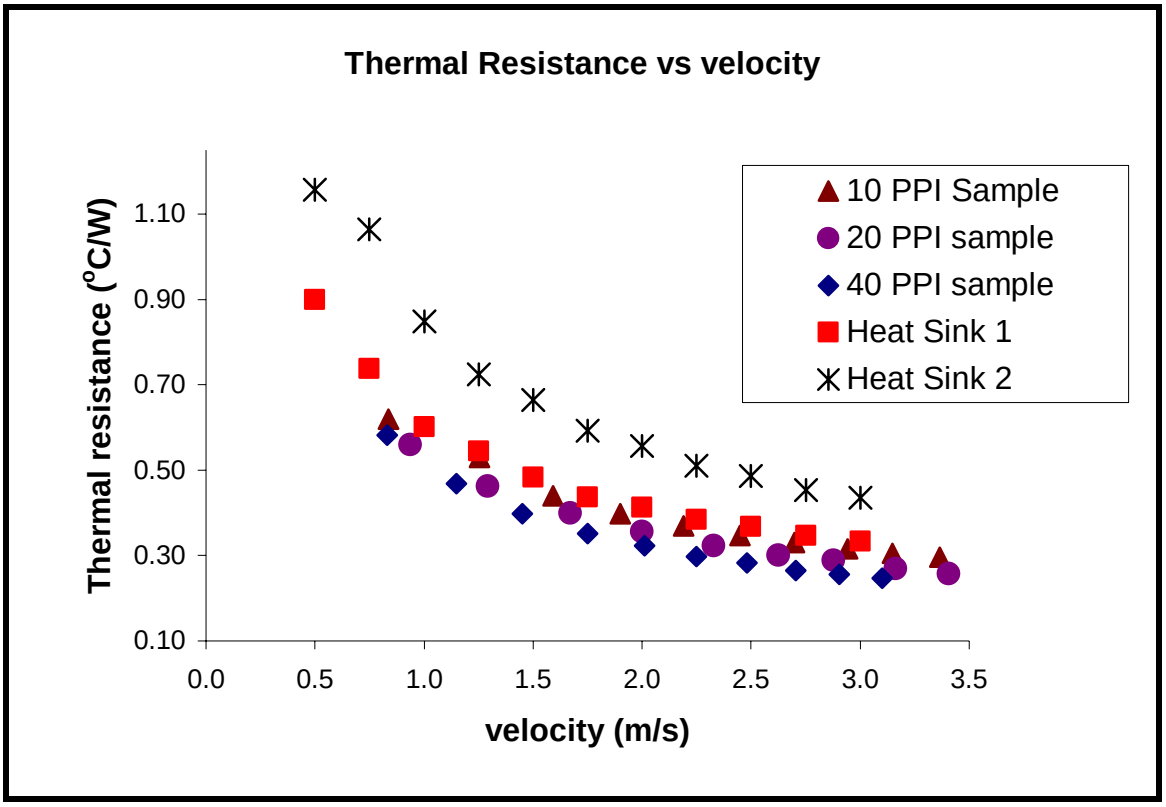

Figure 5.8 Thermal resistance comparison plot

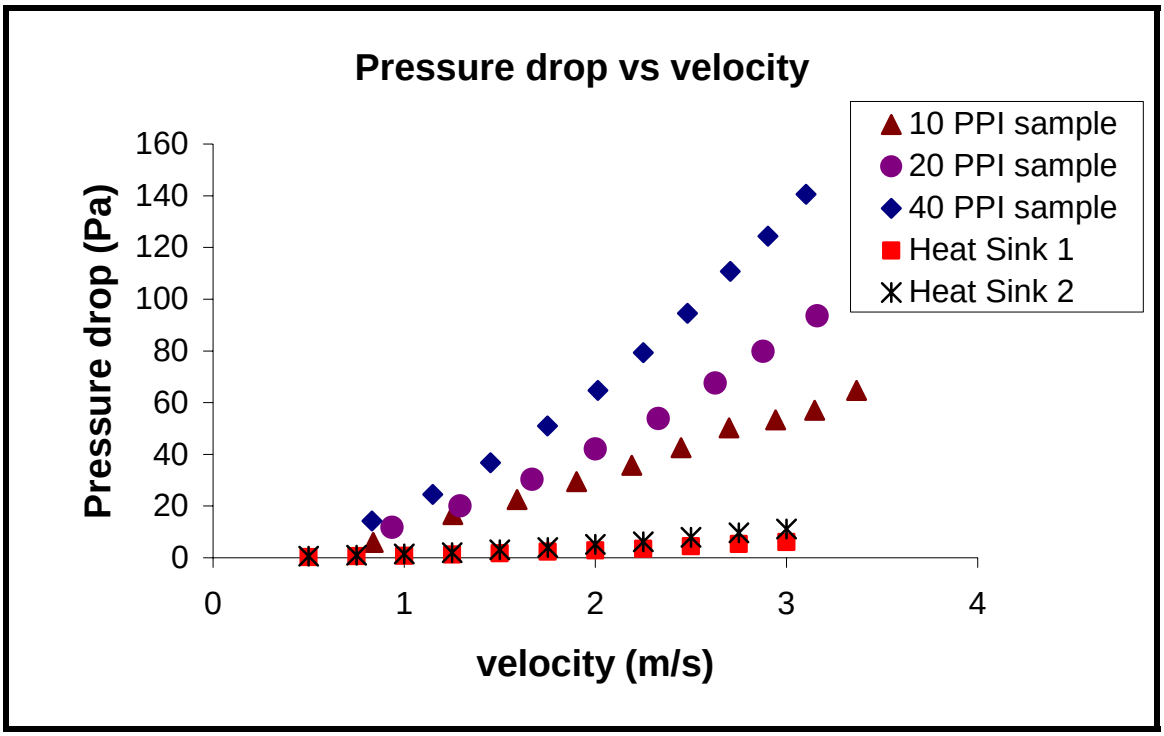

Figure 5.9 Pressure drop vs velocity comparison plot

In Fig. 5.8 it could be seen that the metal foam heat sinks provide less thermal resistance than the best heat sink available from Thermaflo. Although there is a pressure drop increase for the use of porous materials as heat sinks, Fig. 5.9, this pressure drop could be compensated by the increase in heat dissipation that the metal foams offer.

In Table 5.4 a comparison of weight for the metal foams and commercially available heat sinks with same base height is made and it is of interest to find that a weight reduction in the range of 6 to 30 percent can be achieved.

Table 5-4 Weight comparison among commercially available and metal foam heat sinks

Heat Sink	Weight (oz)
P817151B00002	7.1
P696637B00002	5.3
10 PPI metal foam	4.97
20 PPI metal foam	4.97
40 PPI metal foam	4.97

Further in this experimental work a comparison of longitudinal heat sinks of the same dimension and material is obtained with the use of longitudinal fin correlations mentioned in section 4.1 (Lau and Mahajan [39]) and theory of extended surfaces and internal flows. Figs. 5.10 and 5.11 show the comparison of the convection coefficient and pressure drop for a 6 finned heat sink.

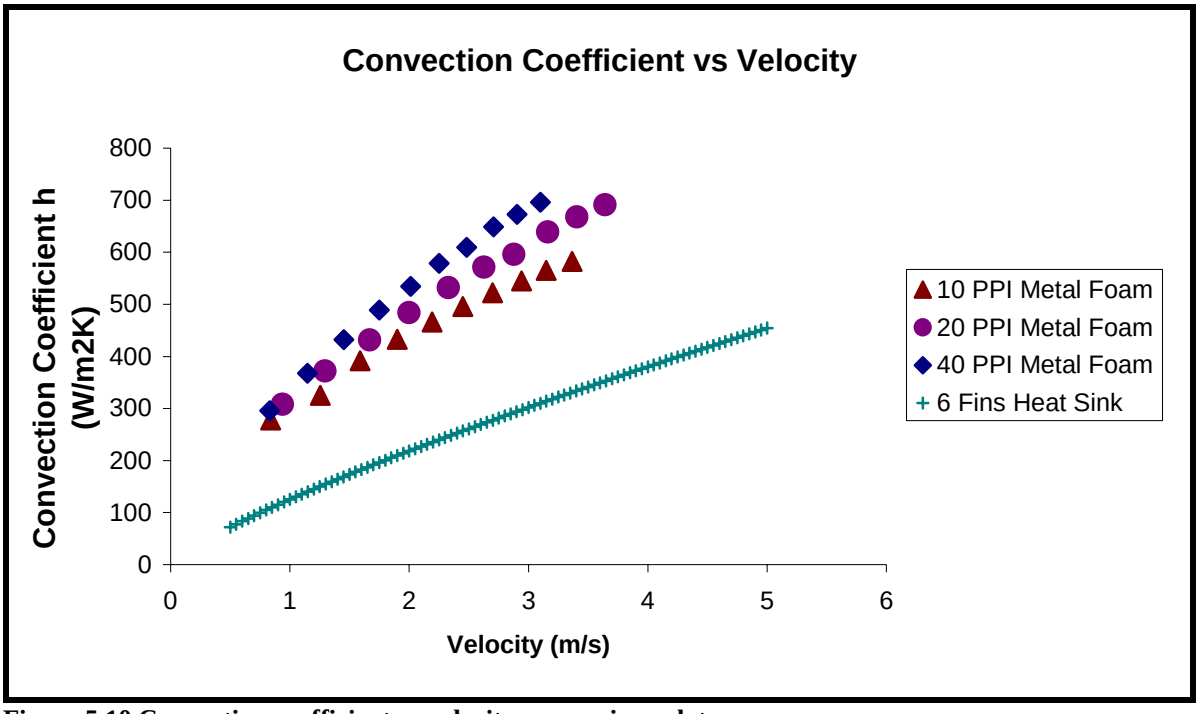

Figure 5.10 Convection coefficient vs velocity comparison plot

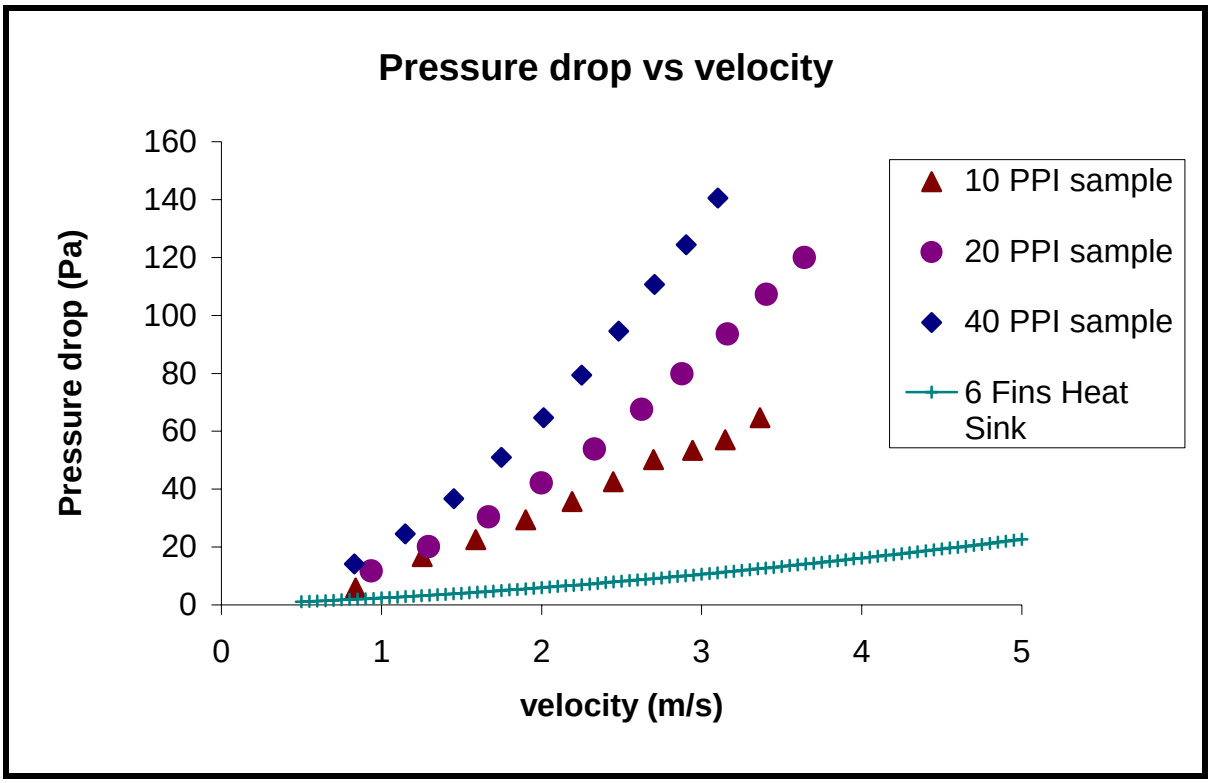

Figure 5.11 Pressure drop vs velocity comparison plot

Two commercially available 12-24 V muffin fans are used in this part of the result in order to compare the heat transfer performance of both longitudinal finned heat sinks and the metal foam samples. The comparison will be made at the operation point based on the fan characteristic curve. Table 5.5 describes the muffin fans used for the comparison and Fig 5.12 is a picture of the fan base model.

Table 5-5 Fan operation data

Model	Nominal voltage (V)	Nominal Air Flow (CFM)	Nominal Pressure (Pa)	Nominal Speed (RPM)
Flight II 90 (FN12B3)	12	45	45.29	2784
Flight II 90 (FN24K3)	24	60	83.36	3750

Figure 5.12 Commercially available muffin fan used for comparison

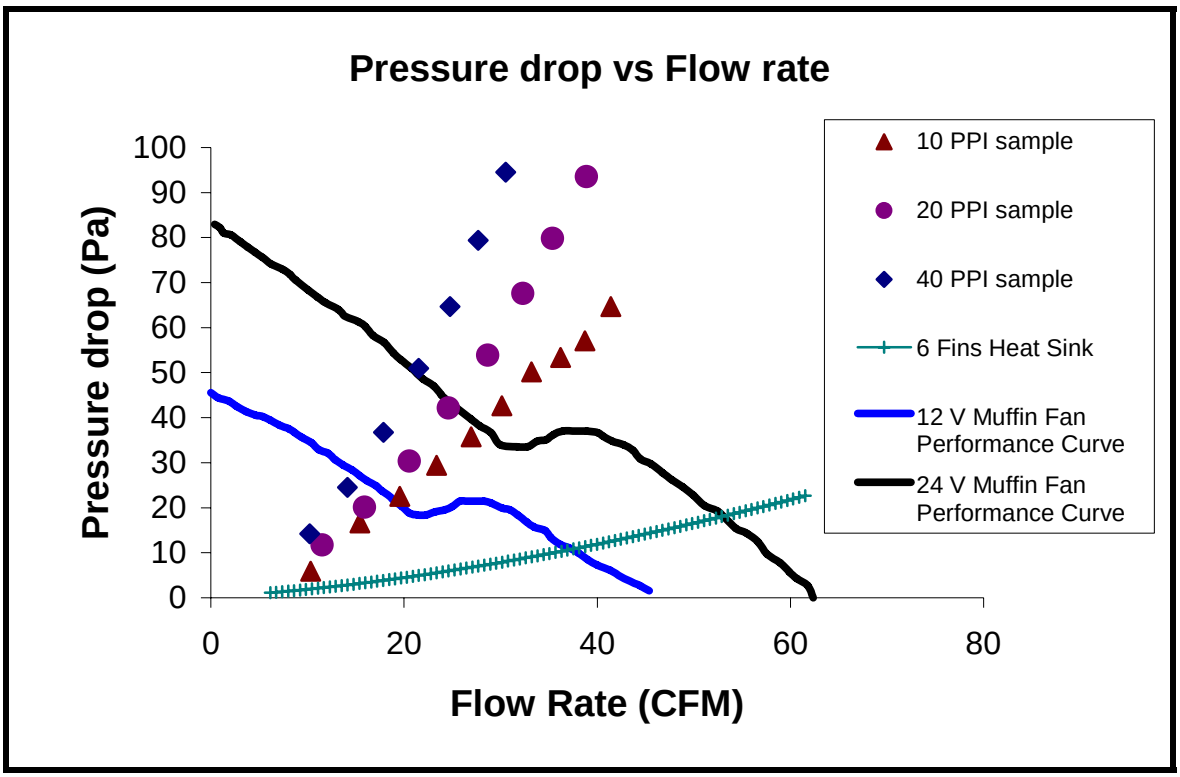

Figure 5.13 System curve for the different heat sinks and the characteristics fan curves

In Fig. 5.13 the operation point of both longitudinal heat sinks and metal foams are obtained. It is noticeable in the operating points of the curve the value of the heat transfer coefficient is higher for the metal foam samples than the longitudinal heat sinks. Table 5.6 shows a summary of the results.

	12 V Fan Convection coefficient (W/m2 K)	**24 V fan Convection coefficient (W/m2 K)**	**Sample Weight (oz)**
10 PPI metal foam	376.41	463.16	6.24
20 PPI metal foam	394.67	473.80	6.24
40 PPI metal foam	398.17	476.99	6.24
6 Fin Heat Sink	298.12	405.48	8.371

Table 5-6 Heat transfer coefficient based on fan curve

Finally the last part of this section will make use of the simplified analytical model for heat transfer in open cell metal foams cooled by a low conductivity fluid. This local thermal equilibrium temperature model made by Dukhan and Picon [41] and will be validated with a thermal imaging of the forced convection test with the metal foam samples. With this Temperature model a further reduction in area for the Metal Foam Heat Sink is obtained given by the effective area (sample height) needed to dissipate the supplied heat flux. In this model the following non-dimensional parameters are defined below;

$$\Theta_S = \frac{T_s - T_\infty}{T_b - T_\infty} \tag{5.4.1}$$

In this equation T_S is the solid ligament temperature and T_b is the base temperature. This has an analytical solution of the form

$$\Theta_S = 1 - erf(\psi) \tag{5.4.2}$$

The similarity transform ψ is described by the following parameters

$$\psi = \frac{\eta}{2\sqrt{\alpha\chi}} \tag{5.4.3}$$

for which η, χ and α are given by;

$$\eta = y\sqrt{\varepsilon\frac{U}{K}} \tag{5.4.4}$$

$$\chi = \frac{x\varepsilon}{\mathrm{Re}_K\sqrt{K}} \tag{5.4.5}$$

$$\alpha = \frac{k_{seff}}{\varepsilon\mu c_p} \tag{5.4.6}$$

The result of the analytical solution, at 3 inches in the flow direction and an air velocity of 1 m/s, is given in Fig. 5.14. It could be observed that approximately at a value of ψ = 1.75, the solution converges to 0. At this value the corresponding height of the samples would be of 0.83 inches for the 10 PPI sample and 0.71 for the 20 PPI sample.

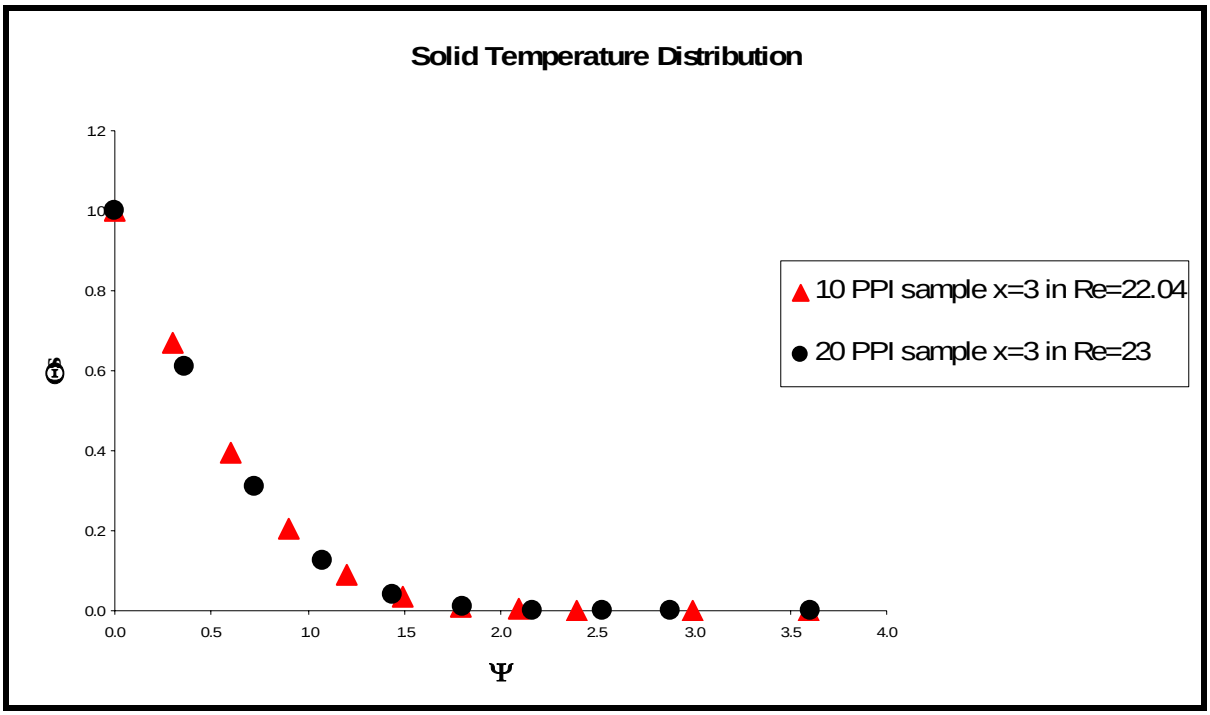

Figure 5.14 Analytical solution of the solid temperature distribution in the metal foam

5.5 Conclusion

One of the primary reasons to study forced convection in metal foams is to provide information necessary for the possible applications of these materials in electronic cooling and other thermal systems. The fibers of these materials could be thought of as a network of complex extended surfaces giving the advantage of increasing the interfacial area. In addition to the increased interfacial area the formation of eddies or fluid mixing promotes the heat transfer enhancement. In this section the results show that;

1. The metal foam heat sinks compared to commercially available heat sinks with similar dimension resulted in a lower thermal resistance.
2. The convection coefficient for a given fan performance curve was increased in a range of 13% to 33%. At a given operation point metal foam heat sinks perform better than the longitudinal fin heat sink.
3. A reduction of weight in the order of 50% was achieved compared with longitudinal heat sinks of the same material.
4. A reduction in transversal area of 72.3% and 76.3% was obtained for the 10 and 20 PPI respectively.

REFERENCES

[1] Ashby, M. F., Evans, A. G., Fleck, N. A., Gibson, L. J., Hutchingson, J. W. and Wadley, H. N. G., 2000, "*Metal Foams, A Design Guide,*" Butterworth-Heinemann, Woburn, MA, Chapter1, also pp. 181-188.

[2] Sullines, D. and Daryabeige, K., 2001. "*Effective Thermal Conductivity of High Porosity Open Cell Nickel Metal Foam,*" Proceedings, 35th AIAA Thermophysics Conference, Anaheim, CA.

[3] Vafai, K and Tien, C. L., 1982 "*Boundary and Inertia Effects on Convective Mass Transfer in Porous Media,*" International Journal of Heat and Mass Transfer, 25(8), pp. 1183-1190

[4] Hwang, J. J., Hwang, G. J., Yeh, R. H. and Chao, C. H., 2002, "Measurements of Interstitial Convective Heat Transfer and Frictional Drag for Flow Across Metal Foams," ASME J. Heat and Mass Transfer, 124, pp. 120-129.

[5] Bhattacharya, A., Calmidi, V. V. and Mahajan, R. L., 2002, "Thermophysical Properties of High Porosity Metal Foams," International Journal of Heat and Mass Transfer, 45, pp. 1017-1031

[6] Kaviany, M., 1995, "*Principles of Heat Transfer in Porous Media",* Second ed., Springer-Verlag, New York, pp 18-51.

[7] Fand, R. M., Kim, B. Y. K., Lam, A. C. C. and Phan, R. T., 1987, ''Resistance to the Flow of Fluids through Simple and Complex Porous Media Whose Matrices are Composed of Randomly Packed Spheres,'' ASME J. Fluids Eng.,**109**, pp. 268–274.

[8] Antohe, B. V., Lage, J. L., Price, D. C. and Weber, R. M., 1997, ''Experimental Determination of Permeability and Inertia Coefficients of Mechanically Compressed Aluminum Porous Matrices,'' ASME J. Fluids Eng., 119, pp. 404–412.

[9] Lage, J. L., Antohe, B. V. and Nield, D. A., 1997, ''Two Types of Nonlinear Pressure-Drop versus Flow-Rate Relation Observed for Saturated Porous Media,'' ASME J. Fluids Eng., **119**, pp. 700–706.

[10] Seguin, D., Montillet, A., Comiti, J. and Huet, F., 1998, ‘‘Experimental Characterization of Flow Regimes in Various Porous Media—II: Transition to Turbulent Regime,’’ Chem. Eng. Sci., 53, pp. 3897–3909.

[11] Macdonald, I. F., El-Sayed, M. S., Mow, K., and Dullien F. A. L., 1979, ‘‘Flow through Porous Media: The Ergun Equation Revisited,’’ Ind. Eng. Chem. Fundam., **18**, pp. 199–208.

[12] Bastawros, A.F., Evans A.G. and Stone H.A., 1999, “Evaluation of Cellular Metal Heat Transfer Media,” Division of Engineering and Applied Sciences. Harvard University. Cambridge, MA 02138.

[13] Bastwros, A. F., 1998, “Effectiveness of Open Cell Metallic Foams for High Power Electronic Cooling,” Presented at the Symposium on the Thermal Management of Electronics, IMECE, Anaheim, CA.

[14] Crosnier, S. Riva, R., Bador, B. and Blet, V., 2003, “Modelling of Gas Flow Through Metallic Foams,” Presented at the 1st European Hydrogen Energy Conference, Sept 2-5, Alpexpo-Alpes Congrés, Grenobel , France.

[15] Khayargoli, P., Loya, V., Lefebvre, L.P., and Medraj, M., 2004, “The Impact of Microstructure on the Permeability of Metal Foams,” CSME 2004 Forum.

[16] Tadrist, L., Miscevic, M., Rahli, O. and Topin, F., 2004, “About the Use of Fibrous Materials in Compact Heat Exchangers,” Exp. Thermal and Fluid Science, vol. 28, pp. 193-199.

[17] Kim, S. Y., Paek, J. W. and Kang, B. H., 2000, “Flow and Heat Transfer Correlations for Porous-Fin Heat Exchangers,” Trans. of the ASME, 122, pp. 572-578.

[18] Paek, J. W., Kang, B. H., Kim, S. Y. and Hyun, J. M., 2000, “Effective Thermal Conductivity and Permeability of Aluminum Foam Materials,” Int. J. of Thermophysics, Vol. 21, No. 2, pp. 453-464.

[19] Du Plessis, J. P., Montillet, A., Comiti, J. and Legrand, J. 1994, “Pressure Drop Prediction for Flow Through high Porosity Metallic Foams,” Chemical Egineering Science, 49, pp. 3545-3553.

[20] Boomsma, K. and Poulikakos, D., 2002, "The Effects of Compression and Pore Size Variations on the Liquid Flow Characteristics in Metal Foams," ASME J. Fluids Eng. 124, pp.263-272.

[21] Boomsma, K., Poulikakos, D. and Zwick, F., 2003, "Metal Foams as Compact High Performance Heat Exchangers," Mechanics of Materials. Vol. 35, pp. 1161-1176.

[22] Diedericks, G. P. J. and Du Plessis, J. P., 1997, ''Modeling of flow through Homogeneous Foams,'' Mathematical Engineering in Industry, Vol. 6, pp. 133–154.

[23] Montillet, A., 2004, "Flow through a Finite Packed Bed of Spheres: A Note on the Limit of the Applicability of the Forchheimer-Type Equation," ASME J. of Fluids Eng., v. 126, p 139-143, 5 p.

[24] Comiti, J., Sabiri, N. E. and Montillet, A., 2000, ''Experimental Characterization of Flow Regimes in Various Porous Media—III: Limit of Darcy's or Creeping Flow Regime for Newtonian and Purely Viscous Non-Newtonian Fluids,'' Chem. Eng. Sci., 55, pp. 3057–3061.

[25] Phanikumar, M.S. and Mahajan, R.L., 2002, "Non-Darcy Natural Convection in High Porosity Metal Foams," Int. Journal of Heat and Mass Transfer, vol. 45, pag. 3781-3793.

[26] Lage, J. and Anthoe, B., 2000, "Darcy's Experiments and the Deviation to Nonlinear Flow Regime," J. of Fluids Eng. Vol .122, pp. 619-625.

[27] Scheidegger, A. E., 1974, "*The Physics of Flows Through Porous Media*," Third ed., University of Toronto Press, Toronto.

[28] Dybbs, A. and Edwards, R. V., 1975, ''Department of Fluid, Thermal, and Aerospace Report,'' presented at Workshop on Heat and Mass Transfer in Porous Media, FTAS/TR ~Case Western Reserve University, Springfield, VA. pp. 75–117.

[29] Givler, R. C. and Altobelli, S. A., 1994, "A Determination of the Effective Viscosity for the Brinkman-Forchheimer Flow Model," Journal of Fluid Mechanics 258: 355-370.

[30] Renken, K. J. and Poulikakos, D., 1988, "Experimental Analysis of Forced Convection Heat Transport in Packed Bed of Spheres," Int. J. Heat Mass Transfer, 31, pp. 1399-1408.

[31] Amiri, A. and Vafai, K., 1994 “Analysis of Dispersion Effect and Nonthermal Equilibrium, Non Darcy Variable Porosity Incompressible Flow through Porous Media,” Int. J. Heat Mass Transfer, 37, pp. 939-954.

[32] Calmidi, V.V. and Mahajan, R. L., 2000, “Forced Convection in High Porosity Metal Foams,” Journal of Heat Transfer. Vol. 122, pp. 557 – 565.

[33] Hunt, M. L. and Tien, C. L., 1988, “Effects of Thermal Dispersion on Forced Convection in Fibrous Media,” International Journal of Heat and Mass Transfer. Vol. 31, pp. 301-309.

[34] Younis, L.B. and Viskanta, R., 1993, “Experimental Determination of the Volumetric Heat Transfer Coefficient Between Stream of Air and Ceramic Foam,” International Journal of Heat and Mass Transfer. Vol. 36, pp. 1425-1434.

[35] Hwang, J.J., Hwang G. J., Yeh, R. H. and Chao, C. H., 2002, “ Measurements of Interstitial Convective Heat Transfer and Frictional Drag for Flow Across Metal Foams,” Trans. ASME, Vol. 124, pp. 120-128.

[36] Boomsma, K. and Poulikakos, D., 2000, “On the Effective Thermal Conductivity of a Three-Dimensionally Structured Fluid-Saturated Metal Foams,” International Journal of Heat and Mass Transfer. Vol. 44, pp. 827-836.

[37] Calmidi, V.V. and Mahajan, R. L., 1999, “The Effective Thermal Conductivity of High Porosity Fibrous Metal Foams,” Trans. ASME, vol. 121, p. 466-471.

[38] Cruz, E., 2004, “Modeling of Heat Transfer in Open Cell Metal Foams,” MS Thesis, University of Puerto Rico, Mechanical Engineering Department.

[39] Lau, K. S., Mahajan, R. L., 1989, “Effects of Tip Clearance and Fin DEnsity on the Performance of Heat links for VLSI Packages,” IEEE Trans. components, Hybrids, and Manufacturing Technology, Vol. 12, No.4, pp. 757-765.

[40] Incropera, F. P., De Witt, D. P., 2002, “Fundamentals of Heat and Mass Transfer,” John Willey & Sons, New York, USA.

[41] Dukhan, N. and Picon, R., 2005, "Simplified Heat Transfer Model Analysis in Metal Foam with Low-Conductivity Fluid," IMECE2005 Proceedings, ASME International Engineering Congress and Exposition, Orlando Florida.

[42] Decker, S., Mößbauer, S., Nemoda, D. T. and Zapf, T., 2000, " Detailed Experimental Characterization and Numerical Modeling of Heat and Mass Transport Properties of Highly Porous Media for Solar Receivers and Porous Burners," Lehrstuhl für Strömungsmechanik Universität Erlangen- Nürnberg Cauerstr. 4, D-91058 Erlangen, Germany.www.lstm.unierlangen.de/ber2/pdf/CleanAir6_numeric.pdf.

[43] Lage, J. L., Antohe, B. V. and Nield, D. A., 1997, ''Two Types of Nonlinear Pressure-Drop versus Flow-Rate Relation Observed for Saturated Porous Media,'' ASME J. Fluids Eng., **119**, pp. 700–706.

[44] Zhao, C. Y., Lu, T.J., Hodson, H.P. and Jackson, J.D., 2004, "The Temperature Dependence of Effective Thermal Conductivity of Open-Celled Steel Alloy Foams," Mat. Science and Eng. A., v. 367, pag. 123-131.

[45] Khayargoli, P., Loya V., Lefebvre, L.P. and Medraj, M., 2004, "The Impact of Microstructure on the Permeability of Metal Foams," CSME forum

[46] Boomsma, K., Poulikakos, D., and Ventikos, Y., 2000, "Simulations of Flow Through Open Cell Metal Foams Using an Idealized Periodic Cell Structure," Int. Journal of Heat and Fluid Flow, vol. 24, pag. 825-834.

[47] Beavers, G. S., and Sparrow, E. M., 1969, ''Non-Darcy Flow Through Fibrous Porous Media,'' ASME J. Appl. Mech., **36**, pp. 711–714.

[48] Nield, D. N. and Bejan, A., 1999, "*Convection in Porous Media*," 2nd ed., Springer-Verlag, New York.

[49] Angirasa D., 2002, "Forced Convective Heat Transfer in Metallic Fibrous Materials," ASME J. Heat Transfer, Vol. 124, pp. 739-745.

[50] Seguin, D., Montillet, A., Comiti, J. and Huet, F., 1998, ''Experimental Characterization of Flow Regimes in Various Porous Media—I: Limits of Laminar Flow Regime,'' Chem. Eng. Sci., 53, pp. 3751–3761.